arXiv:1610.00814v1 [math.DS] 4 Oct 2016

SECOND MINIMAL ORBITS, SHARKOVSKI ORDERING AND UNIVERSALITY IN CHAOS

UGUR G. ABDULLA, RASHAD U. ABDULLA, MUHAMMAD U. ABDULLA, AND NAVEED H. IQBAL

Abstract. This paper introduces the notion of second minimal n-periodic orbit of the continuous map on the interval according as if n is a successor of the minimal period of the map in Sharkovski ordering. We pursue classification of second minimal 7-orbits in terms of cyclic permutations and digraphs. It is proved that there are 9 types of second minimal orbits with accuracy up to inverses. The result is applied to the problem on the distribution of periodic windows within the chaotic regime of the bifurcation diagram of the one-parameter family of unimodal maps. It is revealed that by fixing the maximum number of appearances of the periodic windows there is a universal pattern of distribution. In particular, the first appearance of all the orbits is always a minimal orbit, while the second appearance is a second minimal orbit. It is observed that the second appearance of 7-orbit is a second minimal 7-orbit with Type 1 digraph. The reason for the relevance of the Type 1 second minimal orbit is the fact that the topological structure of the unimodal map with single maximum is equivalent to the structure of the Type 1 piecewise monotonic endomorphism associated with the second minimal 7-orbit. Yet another important report of this paper is the revelation of the universal pattern dynamics with respect to increased number of appearances.

1. Introduction and Main Result

Let $f : I \to I$ be a continuous endomorphism, and I be a non-degenerate interval on the real line. Let $f^n : I \to I$ be an nth iteration of f. A point $c \in I$ is called a periodic point of f with period m if $f^m(c) = c$, $f^k(c) \neq c$ for $1 \leq k < m$. The set of m distinct points

$$c, f(c), \cdots, f^{m-1}(c)$$

is called the orbit of c, or briefly m-orbit or periodic m-cycle. In his celebrated paper [15], Sharkovski discovered a law on the coexistence of periodic orbits of continuous endomorphisms on the real line.

Theorem 1.1 (Sharkovskii)**.** [15] *Let the positive integers be totally ordered in the following way:*

$$1 \triangleleft 2 \triangleleft 2^2 \triangleleft 2^3 \triangleleft \cdots \triangleleft 2^2 \cdot 5 \triangleleft 2^2 \cdot 3 \triangleleft \cdots \triangleleft 2 \cdot 5 \triangleleft 2 \cdot 3 \triangleleft \cdots \triangleleft 9 \triangleleft 7 \triangleleft 5 \triangleleft 3. \tag{1}$$

If a continuous endomorphism, $f : I \to I$, has a cycle of period n and $m \triangleleft n$, then f also has a periodic orbit of period m.

This result played a fundamental role in the development of the theory of discrete dynamical systems. A conceptually novel proof was given in [5]. Following the standard approach, we characterize each periodic orbit with cyclic permutations and directed graphs of transitions or *digraphs*. Consider m-orbit:

$$\mathbf{B} = \{\beta_1 < \beta_2 < \cdots < \beta_m\}$$

Definition 1.2. If $f(\beta_i) = \beta_{s_i}$ for $1 \leq s_i \leq m$, with $i = 1, 2, ..., m$, then $\mathbf{B}$ is associated with cyclic permutation

$$\pi = \begin{bmatrix} 1 & 2 & \dots & m \\ s_1 & s_2 & \dots & s_m \end{bmatrix}$$

Department of Mathematics, Florida Institute of Technology, Melbourne, FL 32901 (abdulla@fit.edu, http://my.fit.edu/~abdulla/).
This work was funded by the NSF grant #1359074: REU Site on PDEs & Dynamical Systems.

Definition 1.3. Let ω be the order reversing permutation

$$\omega = \begin{bmatrix} 1 & 2 & \dots & m-1 & m \\ m & m-1 & \dots & 2 & 1 \end{bmatrix}$$

Then, given a cyclic permutation π, it's inverse is obtained as $\pi^{-1} = \omega \circ \pi \circ \omega$.

In the sequel $< a, b >$ means either $[a, b]$ or $[b, a]$.

Definition 1.4. Let $J_i = [\beta_i, \beta_{i+1}]$. The digraph of m-orbit is a directed graph of transitions with vertices $J_1, J_2, \cdots, J_{m-1}$ and oriented edges $J_i \to J_s$ if $J_s \subset < f(\beta_i), f(\beta_{i+1}) >$.

Definition 1.5. The inverse digraph of m-orbit is a digraph associated with inverse cyclic permutation π^{-1}. Equivalently, inverse digraph is obtained from the digraph of m-orbit by replacing each J_i with J_{m-i}.

Proof of the Sharkovskii's theorem significantly uses the concept of *minimal orbit*.

Definition 1.6. n-orbit of f is called minimal if n is the minimal period of f in Sharkovski's ordering.

Definition 1.7. Digraph of the m-orbit contains the red edge $J_i \to J_s$ if $J_s =< f(\beta_i), f(\beta_{i+1}) >$.

The structure of the minimal orbits is well understood [16, 2, 3, 4]. Minimal odd orbits are called Stefan orbits, due to the following characterization:

Theorem 1.8 (Stefan)**.** [16, 4] *The digraph of a $m = 2k+1$ minimal odd orbit has the unique structure given in Figure 1 up to an inverse.*

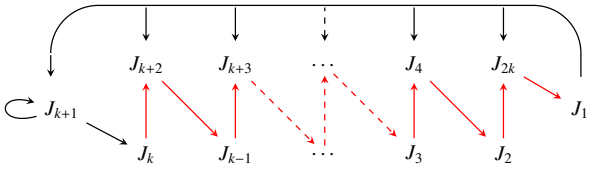


FIGURE 1. Digraph of Minimal Odd Orbit

Similar characterization of $2(2k+1)$-orbits ($k > 1$) is given in [1].

Theorem 1.9. [1] *The digraph of a minimal $2(2k+1)$-orbit ($k > 1$) has one of four types up to their inverses (Type I is shown in Figure 2).*

The main idea of the constructive proof of [1] is based on the fact that each half of the minimal $2(2k+1)$-orbit is minimal $2k+1$ orbit of f^2. Therefore, the digraph of the minimal $2(2k+1)$-orbit is designed as one of the possible four "unions" of two Stefan digraphs of f^2. The result of Theorem 1.9 can be generalized as follows:

Theorem 1.10. *The digraph of any minimal $2^n(2k+1)$-orbit, $k > 1$, has one of $2^{2^{n+1}-2}$ types up to their inverses. Furthermore, each digraph is strongly simple and can be constructed from the digraphs of two minimal and strongly simple $2^{n-1}(2k+1)$-orbits in f^2.*

The main goal of this paper is the characterization of second minimal odd orbits.

Definition 1.11. An n-orbit, $n \geq 7$, of f is called second minimal if n is the successor of the minimal orbit of f in the Sharkovskii ordering.

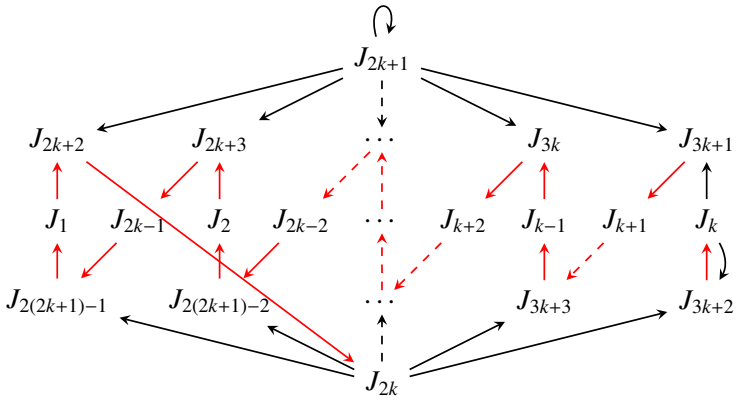


FIGURE 2. Type I digraph of minimal $2(2k+1)$-orbit

$$\begin{pmatrix} 1&2&3&4&5&6&7\\ 4&5&7&6&3&2&1 \end{pmatrix}^1 \quad \begin{pmatrix} 1&2&3&4&5&6&7\\ 3&7&5&6&4&2&1 \end{pmatrix}^2 \quad \begin{pmatrix} 1&2&3&4&5&6&7\\ 6&4&7&5&3&2&1 \end{pmatrix}^3$$
$$\begin{pmatrix} 1&2&3&4&5&6&7\\ 7&4&6&5&3&1&2 \end{pmatrix}^4 \quad \begin{pmatrix} 1&2&3&4&5&6&7\\ 4&6&7&5&2&3&1 \end{pmatrix}^5 \quad \begin{pmatrix} 1&2&3&4&5&6&7\\ 4&6&7&5&3&1&2 \end{pmatrix}^6$$
$$\begin{pmatrix} 1&2&3&4&5&6&7\\ 4&7&6&5&2&1&3 \end{pmatrix}^7 \quad \begin{pmatrix} 1&2&3&4&5&6&7\\ 3&7&6&5&2&4&1 \end{pmatrix}^8 \quad \begin{pmatrix} 1&2&3&4&5&6&7\\ 4&7&5&6&2&3&1 \end{pmatrix}^9$$

TABLE 1. All Second Minimal 7 cycles

For example, if map has a second minimal 7-orbit, then it has a minimal 5-orbit, but no 3-orbit. Our main result reads:

Theorem 1.12. *The second minimal* 7*-orbit has one of* 9 *possible types up to their inverses. The associated cyclic permutations are listed in Table 1; digraphs and piecewise linear representatives are demonstrated in Appendix 1.*

The method of the proof of Theorem 1.12 is extended to prove that the second minimal 9, 11, and 13 orbits have respectively 13, 17, and 21 possible types up to their inverse. We conjecture the following result:

Conjecture 1.13. *The digraph of any second minimal* $(2k+1)$*-orbit,* $k \geq 3$*, has one of* $4k-3$ *possible types up to their inverses.*

We adress the proof of the Conjecture 1.13 in a forthcoming paper.

The structure of the remainder of the paper is as follows: In Section 2, we recall some preliminary facts. Theorem 1.12 is proved in Section 3. In Section 4, we describe a new universal law of the distribution of periodic windows within the chaotic regime of the bifurcation diagram of the one-parameter family of unimodal maps. First we recall the celebrated Feigenbaum scenario of the transition from periodic to chaotic behaviour through successful period doublings and outline the rigorous universality theory in the class of $\mathscr{C}^1$-unimodal maps [8, 6, 7]. In subsection 4.1, we report the numerical reslts which reveal fascinating pattern of distribution of all the superstable periodic orbits when parameter changes in the range between the Feigenbaum transition point to chaos and the value when superstable 3-orbit appears for the first time.

In fact, this parameter range is divided into infinitely many Sharkovski s-blocks where all the $2^s(2k+1)$-orbits are distributed and the pattern is independent of s. Subsection 4.2 demonstartes that the convergence of the successive parameter values for superstable $2^s(2k+1)$-orbits within each s-block is exponential with the rate which is independent of the appearance index. Finally, in subsection 4.3, we report the numerical results which demonstrate that any superstable odd orbit in the indicated parameter range is going through successful period doublings according to the Feigenbaum scenario when the parameter decreases to a critical transition point. This indicates that Feigenbaum Universality is true in more general classes of maps, which are the $(2k+1)$st iteration of the class of $\mathscr{C}^1$-unimodal maps. We end Section 4 with the brief outline of the anticipated rigorous universality theory in general classes of maps.

2. Preliminary Results

Lemma 2.1. *The digraph of an m-orbit,* $\mathbf{B} = \{\beta_1 < \beta_2 < \cdots < \beta_m\}$, $m > 2$, *possesses the following properties* [4]*:*

1. *The digraph contains a loop:* $\exists r_*$ *such that* $J_{r_*} \to J_{r_*}$.
2. $\forall r$, $\exists r'$ *and* r'' *such that* $J_{r'} \to J_r \to J_{r''}$*; moreover, it is always possible to choose* $r' \neq r$ *unless* m *is even and* $r = m/2$, *and it is always possible to choose* $r'' \neq r$ *unless* $m = 2$.
3. *If* $[\beta', \beta''] \neq [\beta_1, \beta_m]$, $\beta', \beta'' \in \mathbf{B}$, *then* $\exists J_{r'} \subset [\beta', \beta'']$ *and* $\exists J_{r'} \not\subseteq [\beta', \beta'']$ *such that* $J_{r'} \to J_{r''}$.
4. *The digraph of a cycle with period* $m > 2$ *contains a subgraph* $J_{r_*} \to \cdots J_r$ *for any* $1 \leq r \leq m-1$.

Definition 2.2. A cycle in a digraph is said to be primitive if it does not consist entirely of a cycle of smaller length described several times.

Lemma 2.3 (Straffin)**.** [17, 4] *If* f *has a periodic point of period* $n > 1$ *and it's associated digraph contains a primitive cycle* $J_0 \to J_1 \to \cdots \to J_{m-1} \to J_0$ *of length m, then f has a periodic point y of period m such that* $f^k(y) \in J_k, (0 \leq k < m)$.

3. Proof of Theorem 1.12

Let $f : I \to I$ be a continuous endomorphism that has a 7-orbit which is second minimal. Let $B = \{\beta_1 < \beta_2 < \cdots < \beta_7\}$ be the ordered elements of this orbit; Let $r_* = \max\{i \mid f(\beta_i) > \beta_i\}$. Such an r_* exists since $f(\beta_1) > \beta_1$ and $f(\beta_{2k+1}) < \beta_{2k+1}$. So, we have a loop: $J_{r_*} \to J_{r_*}$; Let

$$B^- = \{\beta \in B \mid \beta \leq \beta_{r_*}\}, \quad B^+ = \{\beta \in B \mid \beta > \beta_{r_*}\}.$$

Then, $|B^-| + |B^+| = 7$, where $|X|$ denotes the number of elements of the set X. Hence, $|B^-| \neq |B^+|$. Assume that $|B^-| > |B^+|$. Then let $r = \max\{i < r_* \mid f(\beta_i) \leq \beta_{r_*}\}$ so $f(\beta_r) \leq \beta_{r_*}$; $f(\beta_{r+1}) > \beta_{r_*} \Rightarrow J_r \to J_{r_*}$. According to Lemma 2.1 there is a subgraph

$$\circlearrowleft J_{r_*} \to \cdots \to J_r \to J_{r_*} \tag{11}$$

Assume that this is the shortest path. Then its length is at most 7, since there are 6 different intervals, and if any interval is repeated twice, one can get shorter path by removing all the intervals between the repetitions (including one of the repetitions). From another side the length is at least 5, since if it is 4 we will deduce by Lemma 2.3 the existence of 3-orbit. The same conclusion is true if the length is shorter than 4, since if necessary we can always add J_{r_*} to the right end of the subgraph (11). Hence, the length can be 5, 6, or 7; In the sequel $< a, b >$ indicates either $[a, b]$ or $[b, a]$; $\begin{matrix} a \\ b \end{matrix}$ or $a \wedge b$ imply either of the entries a or b are valid choices for mappings of a given node; $J_{r_i} \to [a, b]$ means $f(\beta_{r_i}) = a$ and $f(\beta_{r_{i+1}}) = b$.

Case 1 length is 7 $\Rightarrow$ all 6 intervals are represented in the cycle (11). Choose $r_1 = r_*$, $r_6 = r$ and write

$$\circlearrowleft J_{r_1} \to J_{r_2} \to J_{r_3} \to J_{r_4} \to J_{r_5} \to J_{r_6} \to J_{r_1} \tag{12}$$

Since $\circlearrowleft J_{r_1} \to J_{r_2}$, but $J_{r_1} \nrightarrow J_{r_j}$, $j = 3, \cdots, 6 \Rightarrow J_{r_2}$ must be adjacent to J_{r_1}, so either Figure 3 or Figure 4 is relevant.

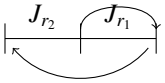


FIGURE 3. Case 1.1

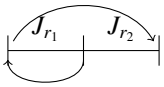


FIGURE 4. Case 1.2

Continuing in this manner we get either Figure 5 or Figure 6. Both are Stefan orbits, and the first one is the right one satisfying $|B^-| = 4 > 3 = |B^+|$, while the second one is its inverse satisfying $|B^+| = 4 > 3 = |B^-|$. But Stefan orbit excludes 5-orbit and so we dismiss this case as irrelevant.

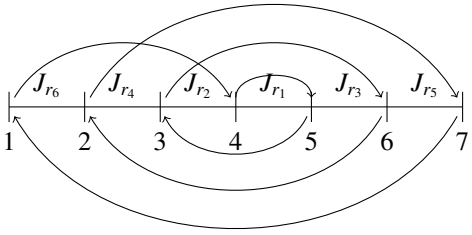


FIGURE 5. Case 1.1

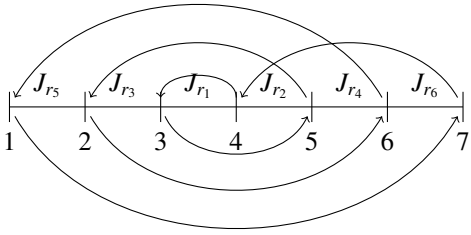


FIGURE 6. Case 1.2

Case 2 length is 6; Choose $r_1 = r_*$, $r_5 = r$ and write

$$\circlearrowleft J_{r_1} \to J_{r_2} \to J_{r_3} \to J_{r_4} \to J_{r_5} \to J_{r_1} \tag{13}$$

We have

$$J_{r_1} \to J_{r_1}, J_{r_1} \to J_{r_2}, J_{r_1} \nrightarrow J_{r_3}, J_{r_4}, J_{r_5} \tag{14a}$$

$$J_{r_2} \to J_{r_3}, J_{r_2} \nrightarrow J_{r_1}, J_{r_4}, J_{r_5} \tag{14b}$$

$$J_{r_3} \to J_{r_4}, J_{r_3} \nrightarrow J_{r_1}, J_{r_5} \ (J_{r_3} \to J_{r_4} \text{ optional}) \tag{14c}$$

$$J_{r_4} \to J_{r_5}, J_{r_4} \nrightarrow J_{r_1}, J_{r_2} \ (J_{r_4} \to J_{r_5} \text{ optional}) \tag{14d}$$

$$J_{r_5} \to J_{r_1}, J_{r_5} \nrightarrow J_{r_3} \ (J_{r_5} \to J_{r_2}, J_{r_4} \text{ optional}) \tag{14e}$$

Hence, we have two possible orders among five intervals J_{r_i}, $i = 1 \cdots 5$. Either
Since there are 6 different intervals, only one interval is missing. Let us denote this interval $\tilde{J}$, and try to find its place. We have $J_{r_5} \to J_{r_1}$ but $J_{r_5} \nrightarrow J_{r_3}$. This implies that the missing interval $\tilde{J}$ must be between J_{r_1} and J_{r_3}. Case 2.2 corresponds to $|B^-| > |B^+|$ so we restrict our discussion to this case.

$$\begin{pmatrix} 1 & 2 & 3 & 4_* & 5 & 6 & 7 \\ 3 & & & & 3 & & \\ 4 & < 5, & 7 > & 6 & 4 & 2 & 1 \end{pmatrix} \tag{15}$$

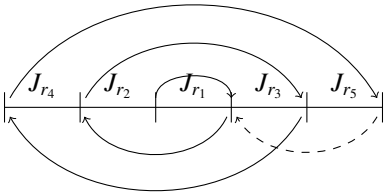


FIGURE 7. Case 2.1, The dashed path demonstrates $J_{r_5} \to J_{r_1}$

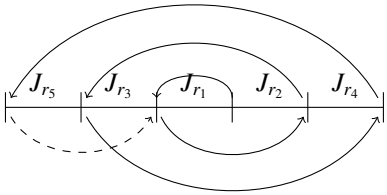


FIGURE 8. Case 2.2, The dashed path demonstrates $J_{r_5} \to J_{r_1}$

Hence, constructing a general cyclic permutation from the rules we have the the 2×7 matrix 15. It follows that either $f(5) = 3$ or $f(5) = 4$. Now, if $f(5) = 3$, according to the rules we must have $f(3) = 7$ and $f(1) = 4$ and this leads to a valid second minimal 7 orbit. Alternatively, if $f(5) = 4$ then we cannot have $f(2) = 5$ else we have a closed 4 cycle. Thus, $f(2) = 7$ and we have a another valid second minimal 7 orbit. Both of these are displayed in Table 1 indexed as 1 and 2 respectively and the digraph for the case $f(2) = 7$ is presented in Figure 9.

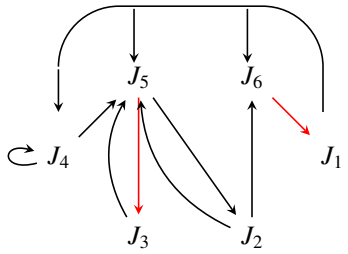


FIGURE 9. Case 2.2 Digraph when $f(2) = 7$

Finally, in order to show that the orbit above is indeed a valid second minimal odd orbit, it must be proven that there are no odd orbits of length less than $2k - 1$. In the case of a second minimal 7 orbit, it must be proven that no 3 orbits are present. Assuming that there is an orbit of length 3, we immediately have two options. Either J_1 is included in the 3 orbit, or it isn't included. If J_1 isn't included, then J_6 can't be included either, because it only maps to J_1. J_4 also can't be included because only J_1 and J_4 map to J_4. If J_1 isn't in the orbit, and J_4 is, then J_4 will only map to itself in the form: $J_4 \to J_4 \to J_4$, as no other orbit will map back to it. The only remaining orbits are $\{J_2, J_3, J_5\}$. Note that these intervals can only form orbits of even length, by splicing together various combinations of the two orbits: $J_3 \to J_5 \to J_3$, and $J_2 \to J_5 \to J_2$. Thus, it is impossible for a 3 orbit to be present in the above digraph, which does not contain J_1.

Suppose now, that the assumed 3 orbit does contain J_1. J_1 can map to either: J_6, J_5, or J_4. If J_1 maps to J_6, the shortest path back to J_1 is: $J_1 \to J_6 \to J_1$, which has a length of 2. If J_1 maps to J_5, the shortest path back to J_1 is $J_1 \to J_5 \to J_2 \to J_6 \to J_1$, which has a length of 4. If J_1 maps to J_4, the shortest path back to J_1 is: $J_1 \to J_4 \to J_5 \to J_2 \to J_6 \to J_1$, which has a length of 5. Thus, it is impossible to form a 3 orbit, regardless if J_1 is or isn't contained. If a 3 orbit is proven impossible,

and a 5 orbit and a 7 orbit where observed during construction of the orbit, then the above cyclic permutation represents a valid second minimal 7 orbit.

It is in this way that the validity of the second minimal orbits are proven. Note that, for all cyclic permutations depicted in Table 1, this same method can be used to effectively prove the fact that no 3 orbits exist. This can also be done by simple observation, as digraphs for a 7 orbit can only have a finite number of interactions.

Case 3 length is 5; (four different intervals are included and two are missing.) Let $r_1 = r_*$, $r_4 = r$, so we have

$$\circlearrowright J_{r_1} \to J_{r_2} \to J_{r_3} \to J_{r_4} \to J_{r_1} \tag{16}$$

then we have

$$J_{r_1} \to J_{r_1}, J_{r_1} \to J_{r_2}, J_{r_1} \nrightarrow J_{r_3}, J_{r_4} \tag{17a}$$

$$J_{r_2} \to J_{r_3}, J_{r_2} \nrightarrow J_{r_1}, J_{r_2}, J_{r_4} \tag{17b}$$

$$J_{r_3} \to J_{r_4}, J_{r_3} \nrightarrow J_{r_1}, J_{r_3} \ (J_{r_3} \to J_{r_2} \text{ optional}) \tag{17c}$$

$$J_{r_4} \to J_{r_1}, J_{r_4} \nrightarrow J_{r_2}, J_{r_4} \ (J_{r_4} \to J_{r_3} \text{ optional}) \tag{17d}$$

So we have either Case 3.1: $J_{r_4}J_{r_2}J_{r_1}J_{r_3}$ or Case 3.2: $J_{r_3}J_{r_1}J_{r_2}J_{r_4}$

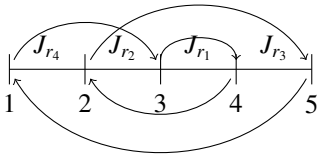


FIGURE 10. Case 3.1, Where we have 3 points in B^-, 2 in B^+; 2 remaining points can't go to B^+

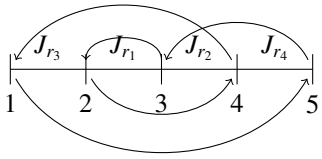


FIGURE 11. Case 3.2, Where we have 2 points in B^-, 3 in B^+; so we need to add both points to B^- and at least one of them should be mapped to B^-.

Consider Case 3.1, where should the remaining intervals go (call them $\tilde{J}$, $\hat{J}$)? Case 3.1.1, assume one is between J_{r_1}, J_{r_3} and the other is between J_{r_4}, J_{r_2}. Now, we adjust Figure 10 in one of the two ways illustrated in Figures 12 and 13.

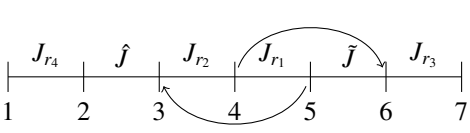


FIGURE 12. Case 3.1.1

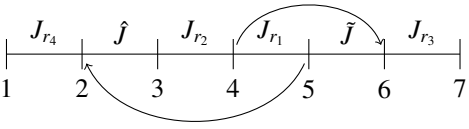


FIGURE 13. Case 3.1.2

Now, we can continue to construct possible orbits graphically in this way and demonstrate which settings for $\hat{J}$ and $\tilde{J}$ result in valid second minimal 7 cycles however, to better communicate the

possible settings, we adopt a slightly different tactic - we will study the cyclic permutations associated with each possible setting in order to extract the relevant cycles. To construct these cyclic permutations first observe in Figures 10 and 11 that there are 5 possible locations in which to insert the extra two intervals $\hat{J}$ and $\tilde{J}$ and we can insert these, assuming we assign $\hat{J}$ first and $\tilde{J}$ second, as demonstrated below in 18:

$$\begin{array}{ccccc} (1,1) & (1,2) & (1,3) & (1,4) & (1,5) \\ & (2,2) & (2,3) & (2,4) & (2,5) \\ & & (3,3) & (3,4) & (3,5) \\ & & & (4,4) & (4,5) \\ & & & & (5,5) \end{array} \tag{18}$$

To construct the cyclic permutation determine where each interval J_{r_i}, $i = 1 \cdots 4$, is mapped to then combine all the mappings. We begin with Case 3.1. We furnish an example of how to construct the cyclic permutation for the setting $(2,4)$ which corresponds to the setting for Figures 12 and 13. First, determine where each interval is mapped according to the rules

$$J_{r_1} = [4,5] \to \begin{bmatrix} 5 & 2 \\ 6, & 3 \end{bmatrix} \quad J_{r_3} = [6,7] \to \left\langle 1, \begin{matrix} 2 \\ 3 \\ 4 \end{matrix} \right\rangle$$

$$J_{r_2} = [3,4] \to \left[7, \begin{matrix} 5 \\ 6 \end{matrix} \right] \quad J_{r_4} = [1,2] \to \left\langle 4, \begin{matrix} 5 \\ 6 \\ 7 \end{matrix} \right\rangle$$

Then, construct the associated cyclic permutation

$$\begin{pmatrix} 1 & 2 & 3 & 4_* & 5 & 6 & 7 \\ < 4, & \begin{matrix} 5 \\ 6 \end{matrix} > & 7 & \begin{matrix} 6 \\ 5 \end{matrix} & \begin{matrix} 2 \\ 3 \end{matrix} & < 1, & \begin{matrix} 3 \\ 2 \end{matrix} > \end{pmatrix} \tag{19}$$

Since $f(3) = 7 \Rightarrow f(7) \neq 3 \Rightarrow f(7) = 1$ or 2.

(a) Case $(2,4)_1$: $f(7) = 1 \Rightarrow$ either $f(6) = 2$, $f(5) = 3$ or $f(6) = 3$, $f(5) = 2$

(b) Case $(2,4)_{1,1}$: $f(7) = 1$, $f(6) = 2$, $f(5) = 3$ or

$$\begin{pmatrix} 1 & 2 & 3 & 4 & 5_* & 6 & 7 \\ < 4, & \begin{matrix} 5 \\ 6 \end{matrix} > & 7 & \begin{matrix} 6 \\ 5 \end{matrix} & 3 & 2 & 1 \end{pmatrix} \tag{20}$$

(c) Case $(2,4)_{1,1,1}$: $f(4) = 6 \Rightarrow J_1 \to J_4$. Now, $f(1) = 5$ implies period 4-suborbit $\{1,3,5,7\}$ which is a contradiction. If $f(1) = 4$ we get the second minimal 7 orbit with index 1 in Table 1.

(d) Case $(2,4)_{1,1,2}$: $f(4) = 5 \Rightarrow$ either $f(1) = 4$, $f(2) = 6$ or $f(1) = 6$, $f(2) = 4$ however since $f(6) = 2$ the former implies a period 2-suborbit $\{2,6\}$ which is a contradiction. The latter case implies the second minimal 7 orbit with index 3 in Table 1.

(e) Case $(2,4)_{1,2}$: $f(7) = 1$, $f(6) = 3$, $f(5) = 2$ or

$$\begin{pmatrix} 1 & 2 & 3 & 4 & 5_* & 6 & 7 \\ < 4, & \begin{matrix} 5 \\ 6 \end{matrix} > & 7 & \begin{matrix} 6 \\ 5 \end{matrix} & 2 & 3 & 1 \end{pmatrix} \tag{21}$$

(f) Case $(2,4)_{1,2,1}$: $f(4) = 6 \Rightarrow f(1) = 5$, $f(2) = 4$. The digraph of the associated cyclic permutation contains the subgraph $J_2 \to J_4 \to J_5 \to J_2$ and by Straffin's lemma this implies the existence of a 3-orbit, a contradiction.

(g) Case $(2,4)_{1,2,2}]$ $f(4) = 5 \Rightarrow$ either $f(1) = 4$ or $f(1) = 6$. The latter implies a period 4-suborbit $\{1,3,6,7\}$, a contradiction. The former implies the second minimal 7 orbit with index 5 in Table 1.

(h) Case $(2,4)_2$: $f(7) = 2 \Rightarrow f(6) = 1$, $f(5) = 3$ or

$$\begin{pmatrix} 1 & 2 & 3 & 4 & 5_* & 6 & 7 \\ < 4, & \begin{matrix} 5 \\ 6 \end{matrix} > & 7 & \begin{matrix} 6 \\ 5 \end{matrix} & 3 & 1 & 2 \end{pmatrix} \tag{22}$$

Considering the alternative we have $f(6) = 1 \Rightarrow f(1) = 5$ or $f(1) = 4$.

(a) Case $(2,4)_{2,1}$: If $f(1) = 5$ the digraph of the associated cyclic permutation contains the subgraph $J_2 \to J_4 \to J_5 \to J_2$ which implies the existence of a 3-orbit, a contradiction.

(b) Case $(2,4)_{2,2}$: $f(1) = 4 \Rightarrow$ either $f(2) = 5$, $f(4) = 6$ or $f(2) = 6$, $f(4) = 5$. In the former case we have a period 4-suborbit $\{2,3,5,7\}$, a contradiction. In the latter case we get the second minimal 7 orbit with index 6 in Table 1.

Now, proceeding in this fashion we will analyze each of the 15 settings to extract valid second minimal 7 orbits.

Setting (1,1) We have the cyclic permutation

$$\begin{pmatrix} 1 & 2 & 3 & 4 & 5_* & 6 & 7 \\ \begin{matrix} 2 \\ 3 \end{matrix} & \begin{matrix} 1 \\ 3 \end{matrix} & 5 & 7 & 6 & 4 & \begin{matrix} 1 \\ 2 \\ 3 \end{matrix} \end{pmatrix} \tag{23}$$

Observe, letting $f(7) = 3$ would force a period 2-suborbit $\{1,2\}$ and period 5-suborbit $\{3,4,5,6,7\}$ so $f(7) = 1$ or $f(7) = 2$ which implies $J_2 \to [1,5]$ or $J_2 \to [3,5]$ both of which lead to the subgraph $J_4 \to J_6 \to J_2 \to J_4$. By Straffin's lemma this implies the existence of a 3-orbit, a contradiction.

Setting (1,2) From 17a and 17b if follows $f(5) = 6$, $f(4) = 7$, from 17a it follows $J_{r_4} = [2,3] \to < 5, 6 \wedge 7 >$ and hence either $f(2) = 6$ or $f(3) = 7$ which is a contradiction since three nodes are mapped to 6 and 7.

Setting (1,3) From 17a and 17b $\Rightarrow f(5) = 6$, $f(6) = 3$, and $J_{r_2} = [3,4] \to < 6, 7 >$ which is a contradiction since three nodes $\{3,4,5\}$ are mapped to $\{6,7\}$.

Setting (1,4) $J_{r_1} = [4,5] \to [5 \wedge 6, 3]$, $J_{r_4} = [2,3] \to [4,7]$, and $J_{r_3} = [6,7] \to < 3 \wedge 4, 1 \wedge 2 >$; Since $f(5) = 3 \Rightarrow$ either $f(6) = 4$ or $f(7) = 4$; but we also have $f(2) = 4$, a contradiction.

Setting (1,5) We have the cyclic permutation

$$\begin{pmatrix} 1 & 2 & 3 & 4_* & 5 & 6 & 7 \\ 2 & & & & & & 2 \\ 6 & 4 & 7 & 5 & 3 & 1 & 1 \\ 7 & & 6 & & & 2 & 6 \end{pmatrix} \tag{24}$$

(i) Case $(1,5)_1$: $f(7) = 6 \Rightarrow f(3) = 7 \Rightarrow f(1) = 2$, and $f(6) = 1$. The digraph of this cyclic permutation contains the subgraph $J_6 \to J_1 \to J_3 \to J_6$ and by Straffin's lemma this implies the existence of a 3-orbit, a contradiction.

(ii) Case $(1,5)_2$: $f(7) = 1 \Rightarrow f(3) = 6$ or $f(3) = 7$

(iii) Case $(1,5)_{2,1}$: $f(7)=1$, $f(3)=6 \Rightarrow f(6)=2$, $f(1)=7$ and this implies the 2-suborbit $\{1,7\}$ and the 5-suborbit $\{2,3,4,5,6\}$.

(iv) Case $(1,5)_{2,2}$: $f(7)=1$, $f(3)=7 \Rightarrow f(6)=2$, $f(1)=6$ and we get the valid second minimal 7-cycle indexed as 3 in Table 1.

(v) Case $(1,5)_3$: $f(7)=2 \Rightarrow f(6)=1$; since $f(1)=6 \Rightarrow$ 2-suborbit $\{1,6\}$ so we must have $f(1)=7$ and $f(3)=6$ and this implies the valid cyclic permutation indexed as 4 in Table 1.

Setting (2,2) From 17b $J_{r_2}=[4,5]\rightarrow[7,6]$ and from 17d $J_{r_4}=[1,2]\rightarrow<5,6\wedge 7>$ which is a contradiction since we have 2 nodes being mapped to 6 and 7.

Setting (2,3) From 17a and From 17b $J_{r_1}=[5,6]\rightarrow[6,2\wedge 3]$ and $J_{r_2}=[3,4]\rightarrow<6,7>$ so $f(5)=6$ and either $f(3)=6$ or $f(4)=6$, a contradiction.

Setting (2,4) See above.

Setting (2,5) We have the cyclic permutation

$$\begin{pmatrix} 1 & 2 & 3 & 4_* & 5 & 6 & 7 \\ <4, & \begin{matrix}6\\7>\end{matrix} & \begin{matrix}7\\6\end{matrix} & 5 & \begin{matrix}2\\3\end{matrix} & 1 & \begin{matrix}3\\2\end{matrix} \end{pmatrix} \tag{25}$$

(i) Case $(2,5)_1$: If $f(5)=3 \Rightarrow f(7)=2 \Rightarrow f(2)\neq 7$ or we have period 2-suborbit $\{2,7\}$. Now, either $f(3)=6$ or $f(3)=7$

(ii) Case $(2,5)_{1,1}$: $f(5)=3$, $f(3)=6 \Rightarrow f(2)=4, f(1)=7 \Rightarrow$ valid second minimal 7-orbit indexed as 4 in Table 1.

(iii) Case $(2,5)_{1,2}$: $f(5)=3$, $f(3)=7 \Rightarrow J_{r_4}=[1,2]\rightarrow<4,6>$.

(iv) Case $(2,5)_{1,1,1}$: $f(5)=3$, $f(3)=7$, $f(2)=6 \Rightarrow f(1)=4 \Rightarrow$ valid second minimal 7-orbit indexed as 6 in Table 1.

(v) Case $(2,5)_{1,1,2}$: $f(5)=3$, $f(3)=7$, $f(2)=4 \Rightarrow f(1)=6 \Rightarrow$ a period 2-suborbit $\{1,6\}$ and a period 5-suborbit $\{2,3,4,5,7\}$, a contradiction.

(vi) Case $(2,5)_2$: If $f(5)=2 \Rightarrow f(7)=3 \Rightarrow f(3)\neq 7$ or we get period 2-suborbit $\{3,7\}$, so $f(3)=6$ and either $f(1)=4$ or 7.

(vii) Case $(2,5)_{2,1}$: $f(5)=2$, $f(7)=3$, $f(3)=6$, $f(1)=4 \Rightarrow$ a valid second minimal cycle indexed as 7 in Table 1.

(viii) Case $(2,5)_{2,2}$: $f(5)=2$, $f(7)=3$, $f(3)=6$, $f(1)=7 \Rightarrow$ period 3-suborbit $\{2,4,5\}$, a contradiction.

Setting (3,3) From 17a, 17b $J_{r_1}=[5,6]\rightarrow[6,2]$ and $J_{r_2}=[2,3]\rightarrow<6,7>$ so $f(5)=6$ and either $f(2)=6$ or $f(3)=6$, a contradiction.

Setting (3,4) We have the cyclic permutation

$$\begin{pmatrix} 1 & 2 & 3 & 4_* & 5 & 6 & 7 \\ \begin{matrix}3\\4\end{matrix} & <\begin{matrix}6\\5,\end{matrix} & 7> & \begin{matrix}5\\6\end{matrix} & 2 & <1, & \begin{matrix}4\\3>\end{matrix} \end{pmatrix} \tag{26}$$

(i) Case $(3,4)_1$: $f(4)=5$ and either $f(1)=3$ or $f(1)=4$.

(ii) Case $(3,4)_{1,1}$: $f(4)=5$, $f(1)=4$ and $f(6)=1$ or 3.

(iii) Case $(3,4)_{1,1,1}$: $f(4)=5$, $f(1)=4$, $f(2)=6$, $f(6)=3 \Rightarrow f(3)\neq 6$ or we get period 2-suborbit $\{3,6\}$, thus $f(3)=7$ giving valid second minimal 7 cycle indexed by 5 in Table 1.

(iv) Case $(3,4)_{1,1,2}$: $f(4)=5$, $f(1)=4$, $f(6)=1 \Rightarrow f(7)=3 \Rightarrow f(3)\neq 7$, or we get period 2-suborbit $\{3,7\}$, thus $f(3)=6$ giving valid second minimal 7 cycle indexed by 7 in Table 1.

(v) Case $(3,4)_{1,2}$: $f(4) = 5$, $f(1) = 3$ and either $f(6) = 1$ or $f(6) = 4$

(vi) Case $(3,4)_{1,2,1}$: $f(4) = 5$, $f(1) = 3$, and $f(6) = 1$ then $f(3) \neq 6$ or we have period 3-suborbit $\{1,3,6\}$ so $f(3) = 7$. Then the digraph of the cyclic permutations has the subgraph $J_1 \to J_3 \to J_5 \to J_1$ and by Straffin's lemma this implies the existence of a period 3-suborbit, a contradiction.

(vii) Case $(3,4)_{1,2,2}$: $f(4) = 5$, $f(1) = 3$, and $f(6) = 4$ then $f(2) \neq 6$ or we have a period 3-suborbit $\{1,3,7\}$ so $f(2) = 7 \Rightarrow$ valid second minimal 7 cycle indexed by 8 in Table 1.

(viii) Case $(3,4)_2$: $f(4) = 6$ and $f(2) = 5 \Rightarrow$ period 2-suborbit $\{2,5\}$ so $f(2) = 7$ and $f(6) = 1$ or $f(6) = 3$ since $f(6) = 4 \Rightarrow$ period 2-suborbit $\{4,6\}$.

(ix) Case $(3,4)_{2,1}$: $f(4) = 6$, $f(2) = 7$, $f(6) = 1 \Rightarrow f(1) = 3$ or $f(1) = 4$.

(x) Case $(3,4)_{2,1,1}$: $f(4) = 6$, $f(2) = 7$, $f(6) = 1$, $f(1) = 3 \Rightarrow$ digraph contains the subgraph $J_1 \to J_3 \to J_5 \to J_1$, a contradiction.

(xi) Case $(3,4)_{2,1,2}$: $f(4) = 6$, $f(2) = 7$, $f(6) = 1$, $f(1) = 4 \Rightarrow$ a period 3-suborbit $\{1,4,6\}$, a contradiction.

(xii) Case $(3,4)_{2,2}$: $f(4) = 6$, $f(2) = 7$, $f(6) = 3 \Rightarrow f(7) = 1 \Rightarrow$ valid second minimal 7 cycle indexed by 9 in Table 1.

Setting (3,5) From 17a, 17b $J_{r_1} = [4,5] \to [5,2]$ and $J_{r_2} = [2,3] \to\!< 5, 6 \wedge 7 >$ so $f(4) = 5$ and either $f(2) = 5$ or $f(3) = 5$, a contradiction.

Setting (4,4) From 17a, 17c, 17d we have $J_{r_1} = [3,4] \to [4 \wedge 5 \wedge 6, 2]$, $J_{r_3} = [6,7] \to\!< 1, 2 \wedge 3 >$, and $J_{r_4} = [1,2] \to [3,7]$. So $f(4) = 2$ and $f(1) = 3$ but either $f(6)$ or $f(7)$ is 2 or 3, a contradiction.

Setting (4,5) From 17a, 17c, 17d we have $J_{r_1} = [3,4] \to [4 \wedge 5, 2]$, $J_{r_3} = [5,6] \to\!< 1, 2 \wedge 3 >$, and $J_{r_4} = [1,2] \to [3, 6 \wedge 7]$. So $f(4) = 2$ and $f(1) = 3$ but either $f(5)$ or $f(6)$ is 2 or 3, a contradiction.

Setting (5,5) We have the cyclic permutation

$$\begin{pmatrix} 1 & 2 & 3_* & 4 & 5 & 6 & 7 \\ 3 & 7 & 4 & 2 & 1 & 5 & 6 \end{pmatrix} \tag{27}$$

The digraph of this cycle admits several subgraphs of length 3; one of which is $J_1 \to J_6 \to J_5 \to J_1$ and by Straffin's lemma this implies a 3-suborbit, a contradiction.

Proceeding in the same fashion for Case 3.2 generates the inverses of the valid cycles already found. Counting all distinct valid second minimal 7 orbits we see there are exactly 9, unique up to an inverse. The topological structure and digraph associated with each of these cyclic permutations are listed in Appendix A.

4. Universality in Chaos

In this section we present some fascinating results pertaining to universal behavior in the route to chaos for a family of unimodal maps. Specifically, we study continuous endomorphisms, dependent on a parameter, from an interval to itself: $f_\lambda : [0,1] \to [0,1]$ satisfying $f(0) = f(1) = 0$ with a single maximum at some point, x_{max}, interior to the interval $[0,1]$ under the iterative relation $x_{n+1} = f_\lambda(x_n)$. We are interested in the asymptotic behavior of x_n for $n \to \infty$ and how this behavior depends on the parameter λ. A prototypical example is the logistic map

$$x_{n+1} = 4\lambda x_n (1 - x_n) \tag{28}$$

In 1978, Fiegenbaum [9, 10, 11] discovered a universal transition mechanism to Chaos through successful period doubling bifurcations. As λ increases, the behaviour of x_n for large n changes from periodic to

chaotic via bifurcations from the 2^n periodic cycle to the 2^{n+1} periodic cycle. Two universal constants $\delta = 4.6692016...$ and $\alpha = -2.502907875...$ qualitatively characterize the universal transition route. Let λ_n^1 be the value of the parameter when 2^n-orbit is superstable, i.e. critical point x_{max} is one of the elements of the orbit, and let d_n^1 be directed distance from x_{max} to the closest element of the orbit:

$$d_n^1 = x_{max} - f_{\lambda_n^1}^{2^{n-1}}(x_{max}).$$

Then $\lambda_n^1 \uparrow \lambda_\infty$, and for a class of unimodal maps with a quadratic maximum of 1 has

$$\lim_{n\to\infty} \frac{\lambda_{n-1}^1 - \lambda_{n-2}^1}{\lambda_n^1 - \lambda_{n-1}^1} = \delta, \quad \lim_{n\to\infty} \frac{d_n^1}{d_{n+1}^1} = \alpha. \tag{29}$$

Having discovered the universality of δ and α numerically, Feigenbaum proposed the mechanism of it based on the renormalization group approach to critical phenomena in statistical mechanics. He revealed that both of these constants are related to a universal function that governs the period doubling route to chaos and expresses this function as the fixed point of some functional operator. The rigorous proof of Feigenbaum's suggested theory was completed for a class of unimodal maps with quadratic maximum in [8, 6, 12]. The following is the brief summary of the rigorous universality theory ([7]).

Map $\psi : [-1, 1] \to [-1, 1]$ is called $\mathscr{C}^1$-unimodal, if $\psi \in C[-1, 1], \psi(0) = 1$; ψ is strictly increasing on $[-1, 0]$ and strictly decreasing on $[0, 1]$; $\psi'(x) \neq 0$ if $x \neq 0$. Let $\mathbb{P}$ be the space of symmetric $\mathscr{C}^1$-unimodal maps. Choose $\psi \in \mathbb{P}$ and define

$$a = a(\psi) = -\psi(1), \; b = b(\psi) = \psi(a).$$

Assume that

$$0 < \psi(b) = \psi^2(a) < a < b < 1. \tag{30}$$

This condition guarantees that the second iteration ψ^2 maps $[-a, a]$ to itself. Therefore, *the doubling transformation*

$$\mathscr{F}\psi(x) = -\frac{1}{a}\psi^2(-ax). \tag{31}$$

maps $[-1, 1]$ to itself. The following properties of $\mathscr{F}$ are key features of the universality theory:

- $\mathscr{F}$ has a fixed point g with $a = -\alpha^{-1}$. Namely, g solves the functional equation

$$g(x) = \alpha g^2\Big(\frac{x}{\alpha}\Big), \quad g(0) = 1. \tag{32}$$

- The Frechet derivative of $\mathscr{F}$ at the fixed point g has a simple eigenvalue equal to δ; the remainder of the spectrum is contained in the open unit disk. Therefore, $\mathscr{F}$ has a one-dimensional unstable manifold W_u and a co-dimension one stable manifold W_s at g.
- W_u intersects transversally the co-dimension one surface Σ_1 of maps with superstable 2-orbits:

$$\Sigma_1 = \{\psi : \psi(1) = 0\}$$

- Consider a set Σ_k of maps with superstable 2^k-orbits (inverse images of Σ_1), i.e.

$$\Sigma_k = \mathscr{F}^{-(k-1)}\Sigma_1 = \{\psi : \psi = \mathscr{F}^{k-1}\phi, \phi \in \Sigma_1\}, \; k = 2, 3, ...$$

  Then the distance between Σ_k and W_s decreases like δ^{-k} for large k.

- Consider an arbitrary one-parameter family $\mu \to \psi_\mu$ of maps and treat it as a curve in $\mathbb{P}$. Assume that this curve crosses the stable manifold W_s at μ_∞ with a non-zero transverse velocity. This implies that for all large k, there will be a unique μ_k near μ_∞, such that $\psi_{\mu_k} \in \Sigma_k$ is a map with superstable 2^k-orbit. Then

$$\lim_{j\to\infty} \mathscr{F}^{j-k}\psi_{\mu_j} = g_k, k = 1, 2, 3, ... \quad \lim_{j\to\infty} \mathscr{F}^j\psi_{\mu_\infty} = g$$

  where g_k is an intersection of Σ_k with W_u; g is a fixed point of $\mathscr{F}$ which solves (32). All the functions g_k and g are universal functions.

The rigorous theory was only developed for a special class of $\mathscr{C}^1$-unimodal maps of the form

$$\psi(x) = f(|x|^{1+\epsilon})$$

where the function f is analytic in a complex neighborhood of $[0, 1]$, $\epsilon > 0$. The typical example would be

$$\psi(x) = 1 - \mu|x|^{1+\epsilon}.$$

The perturbative analysis of [8] requires ϵ to be sufficiently small. The case $\epsilon = 1$ was completed in [6].

In [13] periodic orbits are characterised through patterns, which is the sequence of R's and L's, the kth letter expressing the fact that the kth element of the cycle is on the right or left side of the critical point of the map. In particular, paper [13] presents a table of relative position of periodic orbits of period $p \le 11$ for the logistic map. Much of the work in this direction was inspired by the paper [14], where the calculus for describing the qualitative behaviour of successive iterates of piecewise monotone maps of the interval was invented. We refer to [7] which presents an extensive description of this approach.

In this paper, in addition to the logistic map we will present numerical results for the sine map,

$$f_\lambda(x) = \lambda \sin(\pi x) \tag{33}$$

the cubic map,

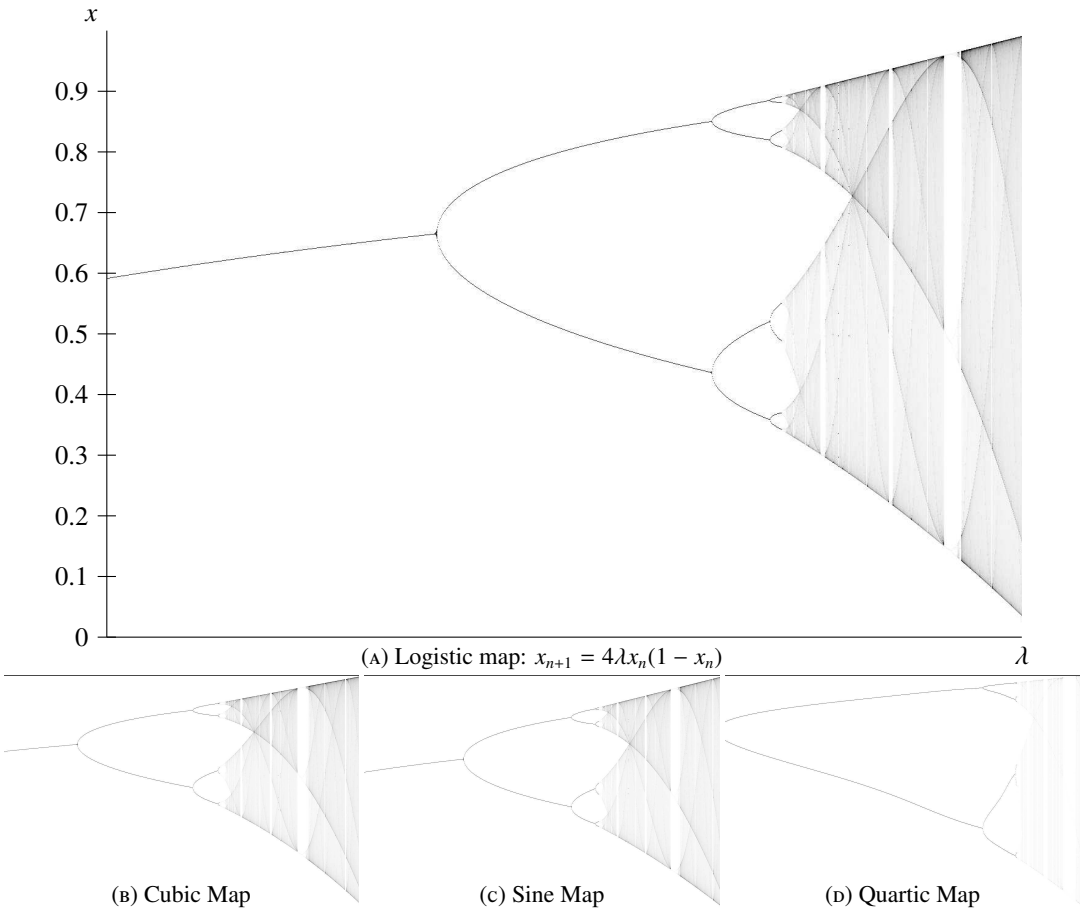
$$f_\lambda(x) = \frac{3\sqrt{3}}{2}\lambda x(1 - x^2) \tag{34}$$

and the quartic map

$$f_\lambda(x) = \lambda - \lambda(2x - 1)^4 f \tag{35}$$

Note that $x_{max} = 0.5$ in (28), (33), (35) and $x_{max} = 1/\sqrt{3}$ in (34). Moreover, only logistic and sine maps are symmetric around x_{max}. All three maps demonstrate Feigenbaum transition route to chaos through successful period doubling from 2^n to 2^{n+1}-orbits. Feigenbaum constants δ and α are the same for logistic, sine and cubic maps. For the quartic map we have $\delta = 7.31...$, and $\alpha = -1.69...$.

It is well-known that for $\lambda > \lambda_\infty$, one can observe all possible periodic orbits within the chaotic regime. Figure 15 demonstrates the *bifurcation diagram* - asymptotic behaviour of the sequence x_n as $n \to +\infty$ (periodic orbits or *chaotic attractors*) as a function of the parameter of the map. One can clearly see periodic windows in the chaotic regime, the period 3 window being the largest. Let $\lambda = \lambda_0^3$ be the value of the parameter when superstable 3-orbit appears first time when $\lambda > \lambda_\infty$ increases. In fact, periodic orbits of all possible periods appear when $\lambda \in [\lambda_\infty, \lambda_0^3]$. Our goal in this section is to continue the results reported in a recent paper [1] and to reveal and analyze a fascinating pattern of distribution of all the periodic windows in this range of the parameter.



(A) Logistic map: $x_{n+1} = 4\lambda x_n(1 - x_n)$

(B) Cubic Map (C) Sine Map (D) Quartic Map

FIGURE 14. Bifurcation Diagrams

4.1. **Ordering in Terms of the Number of Appearences of Orbits.** For any odd number $q > 1$, and nonnegative integer s, let Λ_s^q denotes the set of values $\lambda \in [\lambda_\infty, \lambda_0^3]$ such that f_λ has a superstable $2^s q$-orbit. In fact, the cardinality $|\Lambda_s^q|$ of Λ_s^q is non-zero and finite for all q and s. In particular,

$$\Lambda_0^3 = \{\lambda_0^3\},\ |\Lambda_0^3| = |\Lambda_0^5| = 1,\ |\Lambda_0^7| = 2,\ |\Lambda_0^9| = 4,\ |\Lambda_0^{11}| = 9, ...$$

It is well known that the number of appearances of orbits exponentially increases by increasing the period. Let

$$\Lambda_s^q = \left\{\lambda_{s,1}^q < \lambda_{s,2}^q < \cdots < \lambda_{s,|\Lambda_s^q|}^q\right\},$$

where $\lambda_{s,i}^q$ denotes the value of the parameter which marks the ith appearance of the superstable $2^s q$-orbit when the parameter λ increases in the range $[\lambda_\infty, \lambda_0^3]$. Furthermore this orbit will be called $(2^s q)_i$-orbit. Note that $\lambda_{0,1}^3 = \lambda_0^3$.

Assume that we are looking only first appearance of all the orbits in the indicated parameter range. Numerical results of [1] demonstrate that the first appearances of all the orbits are distributed according to Sharkovskii ordering (1) when parameter λ decreases from λ_0^3 to λ_∞. This is reflected in the first row of the

Table 3. Moreover, the first appearance of all the orbits is always a minimal orbit. For example, the first appearance of all the odd orbits is always a Stefan orbit and its digraph is as in Figure 1 of Theorem 1.8. First appearance of all the $2(2k+1)$-orbits always has Type I digraph as in Figure 2 of Theorem 1.9. The reason of relevance of exactly Type I minimal $2(2k+1)$-orbit is hidden in the fact the topological structure of the unimodal map with single maximum is equivalent to the topological structure of the piecewise monotonic map associated with the Type I digraph of Figure 2. In fact, if we iterate the unimodal map with single minimum then inverse Type I digraph will be relevant.

Assume now that we are looking to first and second appearances of all the $2^s q$-orbits with odd $q \geq 7$, and the first appearance of $2^s q$-orbits with $q = 3, 5$, while the parameter increases from λ_∞ to λ_0^3. Numerical results of [1] and this paper demonstrate the distribution of periodic windows as in (36)-(39). Note that we use a notation $n \leftarrow m$ meaning that parameter decreases from the value giving superstable m-orbit down to the value giving superstable n-orbit.

$$\cdots \leftarrow (2^n 11)_2 \leftarrow (2^n 7)_1 \leftarrow (2^n 9)_2 \leftarrow (2^n 5)_1 \leftarrow (2^n 7)_2 \leftarrow (2^n 3)_1 \leftarrow \cdots \tag{36}$$

$$\vdots$$

$$\cdots \leftarrow 36_1 \leftarrow 44_2 \leftarrow 28_1 \leftarrow 36_2 \leftarrow 20_1 \leftarrow 28_2 \leftarrow 12_1 \leftarrow \cdots \tag{37}$$

$$\cdots \leftarrow 18_1 \leftarrow 22_2 \leftarrow 14_1 \leftarrow 18_2 \leftarrow 10_1 \leftarrow 14_2 \leftarrow 6_1 \leftarrow \cdots \tag{38}$$

$$\cdots \leftarrow 13_2 \leftarrow 9_1 \leftarrow 11_2 \leftarrow 7_1 \leftarrow 9_2 \leftarrow 5_1 \leftarrow 7_2 \leftarrow 3_1 \leftarrow \cdots \tag{39}$$

and we have the pattern $\lambda_{n,1}^{2k-1} < \lambda_{n,2}^{2k+1} < \lambda_{n,1}^{2k-3}$ for $k = 3, 4, \ldots; n = 0, 1, \ldots$ and in particular notice that while decreasing the parameter λ, $(2^s q)$-orbits are changed with respect to q according to pattern $+4-2$; while the index of appearance is changed according to the simple pattern $1, 2, 1, 2, \ldots$. This pattern is expressed in the second row of the Table 3. Interestingly, the second appearance of all the odd orbits is second minimal odd orbit. In fact, this numerically observed fact was a motivation to introduce the notion of second minimal orbit as in Definition 1.11. In fact, in all four maps the second appearance of the 7-orbit is exactly Type I second minimal orbit with cyclic permutation and digraph demonstrated in Table 1 of Theorem 1.12 and Fig. 29 in Appendix. The reason of the relevance of exactly Type 1 second minimal 7-orbit is hidden in the fact that the topological structure of the single maximum unimodal map is equivalent to the topological structure of the piecewise monotonic map associated with Type 1 second minimal 7-orbit of Fig. 29. In fact, according to Theorem 1.12 among all possible 9 types of second minimal 7-orbits (Figures 29-37), Type 1 7-orbit is the only one with a unimodal structure with a single maximum point. In fact, if we iterate the unimodal endomorphism with a single minimum point, then the inverse Type I digraph would be relevant.

Assume now that we are identifying up to third appearances of all the $2^s q$-orbits when the parameter increases from λ_∞ to λ_0^3. Numerical results for all four maps demonstrate the distribution of periodic windows as in (40)-(43).

$$\cdots \leftarrow (2^n 11)_3 \leftarrow (2^n 9)_2 \leftarrow (2^n 5)_1 \leftarrow (2^n 9)_3 \leftarrow (2^n 7)_2 \leftarrow (2^n 3)_1 \leftarrow \cdots \tag{40}$$

$$\vdots$$

$$\cdots \leftarrow 28_1 \leftarrow 44_3 \leftarrow 36_2 \leftarrow 20_1 \leftarrow 36_3 \leftarrow 28_2 \leftarrow 12_1 \leftarrow \cdots \tag{41}$$

$$\cdots \leftarrow 14_1 \leftarrow 22_3 \leftarrow 18_2 \leftarrow 10_1 \leftarrow 18_3 \leftarrow 14_2 \leftarrow 6_1 \leftarrow \cdots \tag{42}$$

$$\cdots \leftarrow 13_2 \leftarrow 9_1 \leftarrow 13_3 \leftarrow 11_2 \leftarrow 7_1 \leftarrow 11_3 \leftarrow 9_2 \leftarrow 5_1 \leftarrow 9_3 \leftarrow 7_2 \leftarrow 3_1 \leftarrow \cdots \tag{43}$$

Note that we have the pattern $\lambda_{n,1}^{2k-1} < \lambda_{n,3}^{2k+3} < \lambda_{n,2}^{2k+1} < \lambda_{n,1}^{2k-3}$ for $k = 3, 4, \ldots; n = 0, 1, \ldots$ and in particular notice that while decreasing the parameter λ, $(2^s q)$-orbits are changed with respect to q according to pattern +4+2-4; while index of appearance is changed according to pattern 1,2,3,... This pattern is expressed in the third row of the Table 3.

Continuing this process reveals the structure presented in Table 3. As an example assume that we are identifying up to 9th appearances of all the $2^s q$-orbits when the parameter increases from λ_∞ to λ_0^3. Numerical results for all four maps demonstrate the distribution of periodic windows according to the pattern expressed in the ninth row of the Table 3. It is satisfactory to explain the pattern only for q-orbits, q is odd number, since the pattern is preserved for $2^n q$-orbits. As it is demonstrated in (44), when the parameter λ decreases from λ_0^3 to λ_∞, superstable q-orbits appear according to pattern +8-2+2-4+4-2+2+2-8 starting with superstable 3-orbit (written in red in (44)), while index of appearance changes according to pattern 1,8,4,7,2,6,3,5,9,...

$$5_1 \overset{-8}{\leftarrow} 13_9 \overset{+2}{\leftarrow} 11_5 \overset{+2}{\leftarrow} 9_3 \overset{-2}{\leftarrow} 11_6 \overset{+4}{\leftarrow} 7_2 \overset{-4}{\leftarrow} 11_7 \overset{+2}{\leftarrow} 9_4 \overset{-2}{\leftarrow} 11_8 \overset{+8}{\leftarrow} 3_1 \tag{44}$$

To construct the table in general, first consider only appearances that are powers of 2. Now, say we wanted to construct the 2^n row of the table, then the two outermost entries, that is, the first and 2^n-th entries are set to $+2(n+1)$ and $-2n$ respectively. Then, the two entries exactly in the middle of the 1st and 2^nth, namely the 2^{n-1}st and $2^{n-1}+1$st entries are set to $-2(n-1)$ and $+2(n-1)$ respectively. Now, find the median entries between the two halves, 1 to 2^{n-1} and $2^{n-1}+1$ to 2^n and set them to $-2(n-2)$ and $+2(n-2)$, and continue in this fashion setting each new set of median entries to $-2(n-i)$ and $+2(n-i)$ for $i = 3, \cdots, n-1$ as illustrated in Figure 15.

To generate the N-th row that is not a power of 2 say $2^n < N < 2^{n+1}$

(1) Find the pattern for 2^n row
(2) Let $J = N - 2^n$
(3) Replace the last J values, $\{p_1, p_2, \cdots, p_j, \cdots, p_J\}$, of the 2^n pattern according to the following rule:
   (a) If $p_j > 0$, $p_j \to \{p_j + 2, -2\}$
   (b) If $p_j < 0$, $p_j \to \{+2, p_j - 2\}$

The procedure to generate the indices is recursive. Given a pattern corresponding to row i of the table to generate the row $i+1$, first counting from 1, left to right, identify the position of i, say it's in position m and insert the new one between positions $m-2$ and $m-1$, unless position $m-1$ is 1, in which case insert the new (highest) index at the end of the list or in the $(i+1)^{th}$ position. For example, to go from row 7 to row 8, we start with row 7 and observe that the highest index, 7, is in position 3 so we insert the new index, 8, in between the index 1 in position 1 and the index 4 in position 2. However, in going from row 8 to row 9 observe that 8 is in position 2 so position $m-1$ is 1. So, we insert 9 at the end of the list in position 9.

4.2. **Constant Shift in Appearences.** Numerical results demonstrate that for all four maps, parameter range $[\lambda_\infty, \lambda_0^3]$ is divided into infinitely many blocks. For arbitrary fixed appearance index $j = 1, 2, ...$ we have

$$\lambda_{s,j}^{2k+1} \downarrow \lambda_s^\infty, \quad as\ k \uparrow \infty;\ s = 0, 1, 2, \ldots, \tag{45}$$

$$\lambda_0^3 > \lambda_0^\infty > \cdots > \lambda_s^\infty > \lambda_{s+1}^\infty > \cdots > \lambda_\infty;\ \ \lambda_s^\infty \downarrow \lambda_\infty, \quad as\ s \uparrow \infty. \tag{46}$$

Note that the limit values λ_s^∞ in (45) are independent of j. Moreover, the results presented in a Table 2 demonstrate exponential convergence in (45):

$$\lambda_{s,j}^{2k+1} - \lambda_s^\infty \sim C\delta_s^{-k}, \quad as\ k \uparrow \infty, \tag{47}$$

where C is some positive constant, and δ_s is a convergence rate. With the notation $\overset{m}{\delta}$ in Table 2, we expressed the fact that m is the highest period of orbit used for the approximation of the convergence rate δ. For example, $\delta_0 = 2.817...$ is calculated for up to a 31-orbit and it is approximately the same up to the 5th appearance of all the odd orbits. This results demonstrates that for any fixed two appearance indices, the ratio of distances of parameter values for respective appearances of superstable $2^s(2k+1)$-orbits is an asymptotically positive constant for large k, i.e. for any fixed positive integers i and j we have

$$\lim_{k\to\infty} \frac{\lambda_{s,j}^{2k+1} - \lambda_s^\infty}{\lambda_{s,i}^{2k+1} - \lambda_s^\infty} = C > 0.$$

TABLE 2. Convergence Rates $\left(\frac{\lambda_{s-1}-\lambda_{s-2}}{\lambda_s-\lambda_{s-1}}\right)$ for $2^s(2k+1)$ orbits

s	Appearance	highest orbit used Convergence Rate			
		Logistic	Sine	Cubic	Quartic
0	1	$\overset{31}{2.81758}$	$\overset{31}{2.93749}$	$\overset{31}{2.96453}$	$\overset{31}{3.95368}$
0	2	$\overset{31}{2.81747}$	$\overset{31}{2.93741}$	$\overset{31}{2.96448}$	$\overset{31}{3.95363}$
0	3	$\overset{31}{2.81734}$	$\overset{31}{2.93731}$	$\overset{31}{2.96437}$	$\overset{31}{3.95362}$
0	4	$\overset{31}{2.81712}$	$\overset{31}{2.93713}$	$\overset{31}{2.96421}$	$\overset{31}{3.95358}$
0	5	$\overset{31}{2.81707}$	$\overset{31}{2.93710}$	$\overset{31}{2.96402}$	$\overset{31}{3.95351}$
1	1	$\overset{30}{2.92338}$	$\overset{38}{2.94158}$	$\overset{38}{2.94044}$	$\overset{38}{4.54383}$
1	2	$\overset{42}{2.95071}$	$\overset{42}{2.93561}$	$\overset{42}{2.93446}$	$\overset{42}{4.53395}$
1	3	$\overset{38}{2.91317}$	$\overset{38}{2.89814}$	$\overset{38}{2.89683}$	$\overset{38}{4.52329}$
1	4	$\overset{34}{2.73591}$	$\overset{34}{2.72223}$	$\overset{34}{2.60199}$	$\overset{34}{4.32894}$
2	1	$\overset{84}{2.94355}$	$\overset{68}{2.93108}$	$\overset{68}{2.93112}$	$\overset{68}{4.40456}$
2	2	$\overset{92}{2.94121}$	$\overset{76}{2.91648}$	$\overset{76}{2.91649}$	$\overset{76}{4.40001}$
2	3	$\overset{100}{2.94257}$	$\overset{84}{2.92619}$	$\overset{84}{2.92622}$	$\overset{84}{4.40308}$
2	4	$\overset{84}{2.94243}$	$\overset{84}{2.92603}$	$\overset{84}{2.92618}$	$\overset{84}{4.40154}$

$$2^n \Big| \; +2(n+1) \underbrace{\quad -2(n-2),\; +2(n-2) \quad}_{2^{n-2}-2} \underbrace{\quad -2(n-1),\; +2(n-1) \quad}_{2^{n-2}-2} \underbrace{\quad -2(n-2),\; +2(n-2) \quad}_{2^{n-2}-2} -2n \; \Big|$$

FIGURE 15. Generation of the 2^n-th row of Table 3

TABLE 3. Pattern of Patterns

Appearance	Pattern	indexes of Appearance
$1 = 2^0$	+2	1
$2 = 2^1$	+4 | −2	1, 2
3	+4 | +2 | −4	1, 2, 3
$4 = 2^2$	+6 | −2 | +2 | −4	1, 4, 2, 3
5	+6 | −2 | +2 | +2 | −6	1, 4, 2, 3, 5
6	+6 | −2 | +4 | −2 | +2 | −6	1, 4, 2, 6, 3, 5
7	+6 | +2 | −4 | +4 | −2 | +2 | −6	1, 4, 7, 2, 6, 3, 5
$8 = 2^3$	+8 | −2 | +2 | −4 | +4 | −2 | +2 | −6	1, 8, 4, 7, 2, 6, 3, 5
9	+8 | −2 | +2 | −4 | +4 | −2 | +2 | +2 | −8	1, 8, 4, 7, 2, 6, 3, 5, 9
10	+8 | −2 | +2 | −4 | +4 | −2 | +4 | −2 | +2 | −8	1, 8, 4, 7, 2, 6, 3, 10, 5, 9
11	+8 | −2 | +2 | −4 | +4 | +2 | −4 | +4 | −2 | +2 | −8	1, 8, 4, 7, 2, 6, 11, 3, 10, 5, 9
12	+8 | −2 | +2 | −4 | +6 | −2 | +2 | −4 | +4 | −2 | +2 | −8	1, 8, 4, 7, 2, 12, 6, 11, 3, 10, 5, 9
13	+8 | −2 | +2 | +2 | −6 | +6 | −2 | +2 | −4 | +4 | −2 | +2 | −8	1, 8, 4, 7, 13, 2, 12, 6, 11, 3, 10, 5, 9
14	+8 | −2 | +4 | −2 | +2 | −6 | +6 | −2 | +2 | −4 | +4 | −2 | +2 | −8	1, 8, 4, 14, 7, 13, 2, 12, 6, 11, 3, 10, 5, 9
15	+8 | +2 | −4 | +4 | −2 | +2 | −6 | +6 | −2 | +2 | −4 | +4 | −2 | +2 | −8	1, 8, 15, 4, 14, 7, 13, 2, 12, 6, 11, 3, 10, 5, 9
$16 = 2^4$	+10 | −2 | +2 | −4 | +4 | −2 | +2 | −6 | +6 | −2 | +2 | −4 | +4 | −2 | +2 | −8	1, 16, 8, 15, 4, 14, 7, 13, 2, 12, 6, 11, 3, 10, 5, 9

4.3. **Feigenbaum Universlity in General Classes.** Numerical results demonstrate that all the odd orbits which appear in the parameter window $(\lambda_0^\infty, \lambda_0^3]$ are going to go through infinitely many period doubling transformations when λ decreases towards λ_∞. This is demonstrated in the diagram (40)-(43) if we consider periods up to 3rd appearances. Let us fix any positive integer J as highest appearance index, and deduce from the Jth row of the Table 3 the distribution of all the odd orbits up to Jth appearance in the parameter window $(\lambda_0^\infty, \lambda_0^3]$ (e.g. if $J = 9$ then the portion of the odd orbits up to 9th appearnces between 3_1 and 5_1 are demonstrated in (44)). All these orbits are going to go through infinitely many bifurcations when λ decreases towarsd λ_∞, and for any positive integer s, the sth bifurcation appears in the parameter window $(\lambda_{s+1}^\infty, \lambda_s^\infty)$. It is fascinating that all these transition routes to chaos follow Feigenbaum universality. In particular, it is revealed that the Feigenbaum universality is relevant in very general classes of maps beyond the unimodal smooth endomorphisms.

Let integers $k \geq 1$ and $j \in [1, |\Lambda_0^{2k+1}|]$ be fixed. Recall that $\lambda_{0,j}^{2k+1}$ is the value of the parameter λ when superstable $(2k+1)$-orbit appears jth time while increasing λ from λ_∞ to λ_0^3. Numerical results demonstrate that for all four maps we have

$$\lambda_{s,j}^{2k+1} \downarrow \lambda_\infty, \quad as\ s \uparrow \infty; \tag{48}$$

$$\lim_{s\to\infty} \frac{\lambda_{s-1,j}^{2k+1} - \lambda_{s-2,j}^{2k+1}}{\lambda_{s,i}^{2k+1} - \lambda_{s-1,j}^{2k+1}} = \delta, \tag{49}$$

$$\lambda_{s,j}^{2k+1} - \lambda_\infty \sim C\delta^{-s}, \quad as\ s \uparrow \infty, \tag{50}$$

where $\delta = 4.6692...$ in the case of logistic, sine and cubic maps (Tables 4, 5, 6); $\delta = 7.31...$ in the case of the quartic map (Table 7); $C > 0$. Hence, we see that the convergence rate of the sequence of parameter values for superstable $(2^s(2k+1))_j$-orbits to critical value λ_∞ as $s \to +\infty$ from above is the same as the convergence rate of the sequence of parameter values for the superstable 2^s-orbits to the same value λ_∞ from below. To clarify if Feigenbaum universality mechanism is indeed relevant we check asymptotical properties of the scaling factor for successful period doublings from $(2^s(2k+1))_j$- to $(2^{s+1}(2k+1))_j$-orbits. Let $d_{s,j}^{2k+1}$ be a directed distance from the maximum point of the map to the closest element of the superstable $(2^{s+1}(2k+1))_j$-orbit, i.e.

$$d_{s,j}^{2k+1} = x_{max} - f_{\lambda_{s+1,j}^{2k+1}}^{2^s(2k+1)}(x_{max}). \tag{51}$$

Numerical results in Tables 4-7 demonstrate that for all four models we have

$$\lim_{s\to\infty} \frac{d_{s-1,j}^{2k+1}}{d_{s,j}^{2k+1}} = \alpha, \tag{52}$$

where $\alpha = -2.5029...$ in the case of logistic, sine and cubic maps (Tables 4, 5, 6); $\alpha = -1.69...$ in the case of the quartic map (Table 7). Hence, we see that the scaling factor of the successive bifurcations of the superstable $(2^s(2k+1))_j$-orbits when λ converges to critival value λ_∞ as $s \to +\infty$ from above is the same as the scaling factor of the successive bifurcations of the superstable 2^s-orbits when λ converges to critical value λ_∞ from below. This indicates that the doubling transformation (31) with scaling factor $a = \alpha$ is a driving force for the transition to chaos through successful bifurcations of superstable $(2^s(2k+1))_j$-orbits for $s = 0, 1, 2, ...$ Therefore, Feigenbaum's universality theory should be valid beyond the class of $\mathscr{C}^1$-unimodal maps - the classes of maps whose structure is defined with qth iteration of unimodal maps, where $q = 2k+1$ is any fixed odd number. Following Feigenbaum [9, 10] define the functions

$$g_m^{2k+1}(x) = \lim_{s\to\infty} (-\alpha)^s\, f_{\lambda_{s+m,j}^{2k+1}}^{2^s(2k+1)}\left(\frac{x}{(-\alpha)^s}\right),\ m = 1, 2, ... \tag{53}$$

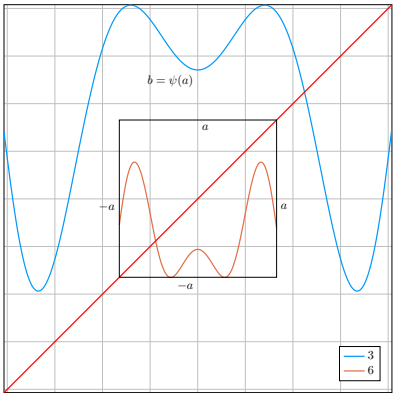


FIGURE 16. Period doubling mechanism for 3_1 showing the scaling

$$g^{2k+1}(x) = \lim_{m\to\infty} g_m^k(x) = \lim_{s\to\infty} (-\alpha)^s f_{\lambda_\infty}^{2^s(2k+1)}\left(\frac{x}{(-\alpha)^s}\right),\ k = 1, 2, ... \tag{54}$$

Numerical results demonstarte that for any fixed non-negative integer k, family of functions in (53), (54) are universal functions. The case $k = 0$ in (53), (54) is a particular case of classical Feigenbaum universality theory explaining the transition from 2^s-orbits, $s = 0, 1, 2, ...$ to chaos through successful period doublings (see (29) and following description of the rigorous universality theory). In this case $g^{(1)} = g$ is a fixed point of the doubling operator $\mathscr{F}$ as in (32); each $g_m^{(1)} = g_m$ is the intersection of Σ_m with the one-dimensional unstable manifold passing through g. Figure 17 demonstrates the convergence to the universal function g_1 in Figure 23(a) for the logistic map after calculation of the few terms under the limit sign in (53).

Figures 18, 19, 20, 21, 22 demonstrate the convergence in (53) to universal functions g_1^{2k+1} via successive bifurcations of superstable $(2^s3)_1$-, $(2^s7)_1$-, $(2^s7)_2$-, $(2^s9)_1$-, $(2^s9)_2$-orbits respectively under the transition (48)-(50) for the logistic map. Note that the side length of the green square in each of the Figures 18-22 is equal to respective value of $d_{s,j}^{2k+1}$, and Figures 23(b),(c), 24(a)(b) demonstrate the first four terms of the limit expression in (53).

In fact, the universal functions $g^{2k+1}, k = 1, 2, ...$ in (54) are fixed points of the doubling operator $\mathscr{F}$, and solve the functional equation in (32). That is the reason that the convergence rate of parameter sequences in (48)-(50) is the same universal constant δ. Moreover, It is easy to prove that if function g solves functional equation (32), then any iteration of g is also a solution of the same equation. The normalization condition $g(0) = 1$ can be arranged by replacing g with $g_\mu = \mu g(x/\mu)$, and by choosing the constant μ appropriately. Indeed, for arbitrary $\mu \neq 0$, g_μ is a solution of the functional equation (53) if g is so. Hence, universal functions g^{2k+1} must be exactly $2k + 1$st iterations of the universal function g (which is the justification of our notation), which is the fixed point of the doubling operator in the class of $\mathscr{C}^1$-unimodal maps. For any fixed $k = 1, 2, ..., g^{2k+1}$ represents a fixed point of the doubling operator (and hence solving the functional equation in (32)) in the more complicated class of maps which is the $(2k + 1)$st iteration of the class of $\mathscr{C}^1$-unimodal maps.

Hence, the numerical analysis suggests that the known rigorous universality theory ([7]) must be true in a much larger class of maps than $\mathscr{C}^1$-unimodal maps, and this generalization is a driving force of infinitely many Feigenbaum scenarios of transition to chaos through successive bifurcations of all possible odd orbits as it is outlined in (48)-(54). We end our presentation with the description of the anticipated rigorous universality theory in the particular case of $k = 1$, or in the class of maps which is the 3rd iteration of the

$\mathscr{C}^1$-unimodal maps. Let

$$\mathbb{P}^3 = \{\phi : \phi = \psi^3, \psi \in \mathbb{P}\}.$$

Assume that $\psi \in \mathbb{P}$ satisfies (30). Since ψ is continuous, there exists $e \in (a, 1)$ such that $\psi(e) = 0$, and ψ^2 is increasing and maps $[0, e]$ onto $[-a, 1]$; ψ^2 is decreasing and maps $[e, 1]$ onto $[b, 1]$. By continuity there exists $d \in (0, a)$ such that $\psi^2(d) = 0$. Now consider symmetric function $\phi = \psi^3$. ϕ is increasing and maps $[0, d]$ onto $[b, 1]$; ϕ is decreasing and maps $[d, e]$ onto $[-a, 1]$; ϕ is increasing and maps $[e, 1]$ onto $[-a, \psi(b)]$; This guarantees that the second iteration $\phi^2 = \psi^6$ maps $[-a, a]$ to itself. Indeed, first of all from (30) it follows that $\phi(a) > b$, and hence, ϕ maps $[-a, a]$ to $[b, 1]$. Also, since ψ^2 maps $[-a, a]$ to itself, we have $\phi(b) = \psi^4(a) \le a$. Accordingly, ϕ maps $[b, 1]$ into $[-a, a]$, and hence ϕ^2 maps $[-a, a]]$ to itself. Therefore, the doubling transformation $\mathscr{F}$ maps $[-1, 1]$ into itself. Figure 16 demonstrates the structure of $\phi = \psi^3$ and $\phi^2 = \psi^6$ under the condition (30).

The following properties of $\mathscr{F}$ are key features of the universality theory in the class $\mathbb{P}^3$:

- $\mathscr{F}$ has a fixed point g^3 with $a = -\alpha^{-1}$. Namely, g^3 solves the functional equation in (32) in the class $\mathbb{P}^3$. In fact, g^3 is precisely 3rd iteration of the fixed point of the doubling operator $\mathscr{F}$ in the class of $\mathscr{C}^1$-unimodal maps, defined in (32).
- The Frechet derivative of $\mathscr{F}$ at the fixed point g^3 has a simple eigenvalue equal to δ; the remainder of the spectrum is contained in the open unit disk. Therefore, $\mathscr{F}$ has a one-dimensional unstable manifold W_u and a codimension one stable manifold W_s at g^3.
- W_u intersects transversally the codimension-one surface Σ_1^3 of maps with superstable 2-orbits:

$$\Sigma_1^3 = \{\phi \in \mathbb{P}^3 : \phi^2(0) = 0\}$$

- Consider a set Σ_m^3 of maps with superstable 2^m-orbits (inverse images of Σ_1^3), i.e.

$$\Sigma_m^3 = \mathscr{F}^{-(m-1)}\Sigma_1^3 = \{\phi : \phi = \mathscr{F}^{m-1}\phi_0, \phi_0 \in \Sigma_1^3\},\ m = 2, 3, ...$$

  Then the distance between Σ_m^3 and W_s decreases like δ^{-m} for large m.
- Consider arbitrary one-parameter family $\mu \to \phi_\mu$ of maps and treat it as a curve in $\mathbb{P}^3$. Assume that this curve crosses stable manifold W_s at μ_∞ with non-zero transverse velocity. This implies that for all large m, there will be a unique μ_m near μ_∞ such that $\phi_{\mu_m} \in \Sigma_m^3$ is a map with superstable 2^m-orbit. Then

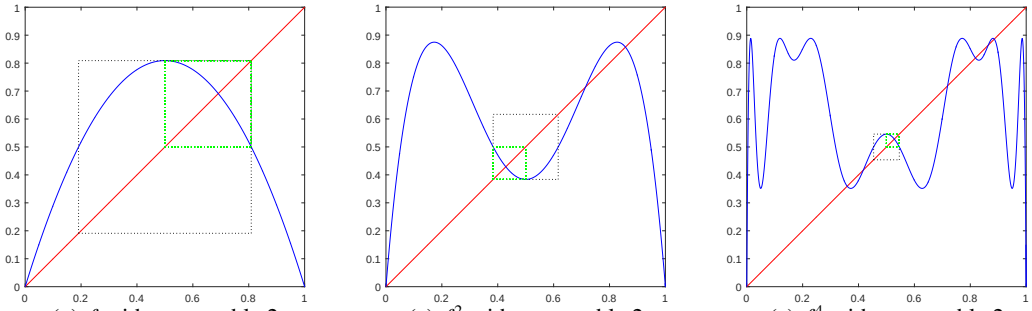
$$\lim_{j\to\infty} \mathscr{F}^{j-m}\phi_{\mu_j} = g_m^3, m = 1, 2, 3, ...\ \lim_{j\to\infty} \mathscr{F}^j\psi_{\mu_\infty} = g^3$$

  where g_m^3 is an intersection of Σ_m with W_u; g^3 is a fixed point of $\mathscr{F}$ which solves functional equation in (32) in the class $\mathbb{P}^3$. All the functions g_m^3 and g^3 are universal functions.

For example, numerical calculation of the universal function g_1^3 is demonstrated in Figure 24(b).

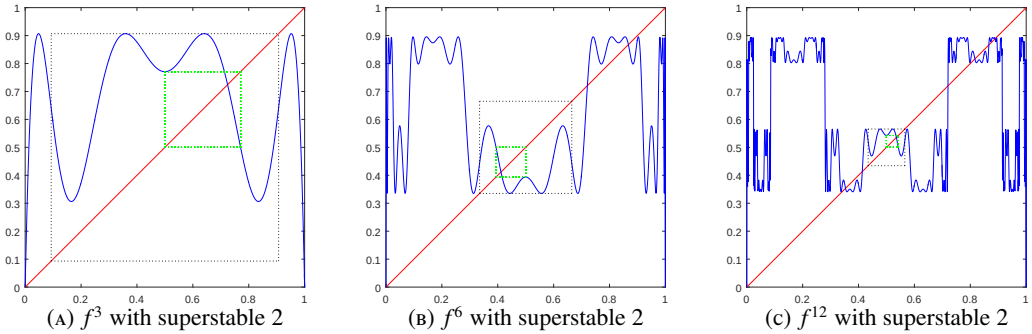
Similar description of the rigorous universality theory can be outlined in various classes

$$\mathbb{P}^{2k+1} = \{\phi : \phi = \psi^{2k+1}, \psi \in \mathbb{P}\},\ k = 2, 3, 4, ...$$



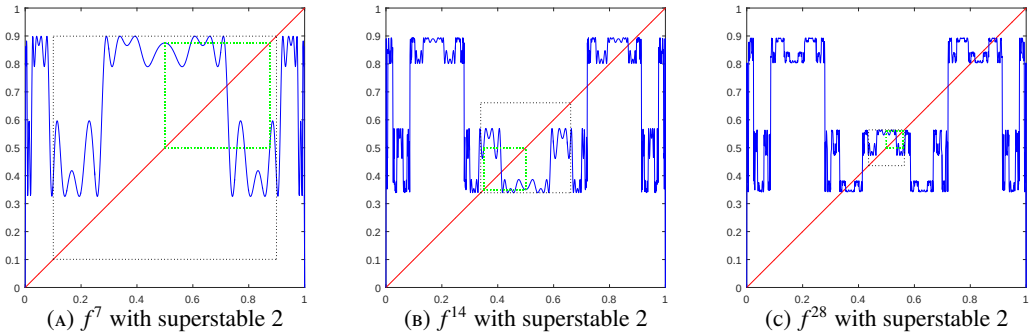
(A) f with superstable 2 (B) f^2 with superstable 2 (C) f^4 with superstable 2

FIGURE 17. The Period Doubling Mechanism



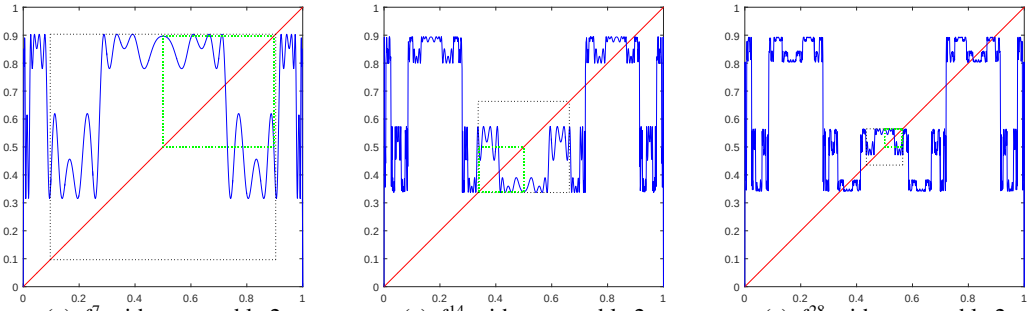
(A) f^3 with superstable 2 (B) f^6 with superstable 2 (C) f^{12} with superstable 2

FIGURE 18. The Period Doubling Mechanism for 3_1



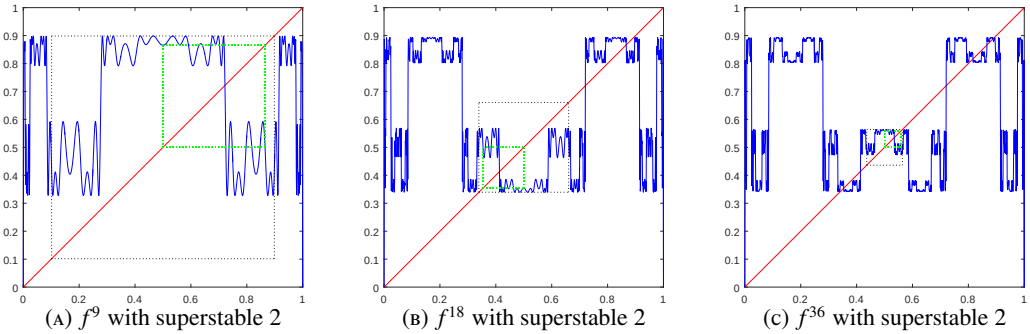
(A) f^7 with superstable 2 (B) f^{14} with superstable 2 (C) f^{28} with superstable 2

FIGURE 19. The Period Doubling Mechanism for 7_1



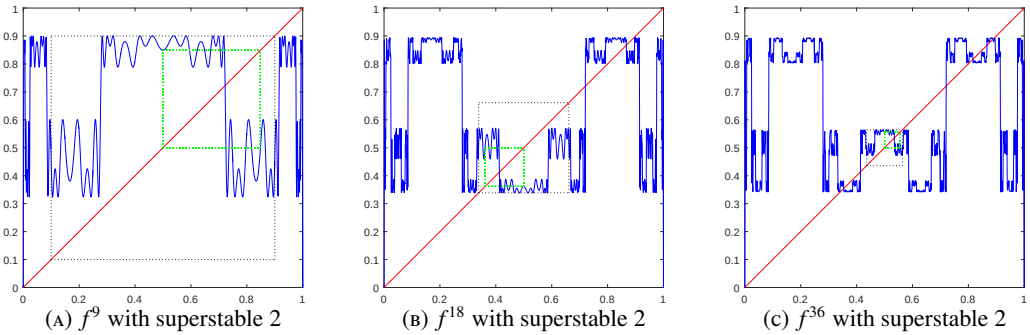
(A) f^7 with superstable 2 (B) f^{14} with superstable 2 (C) f^{28} with superstable 2

FIGURE 20. The Period Doubling Mechanism for 7_2



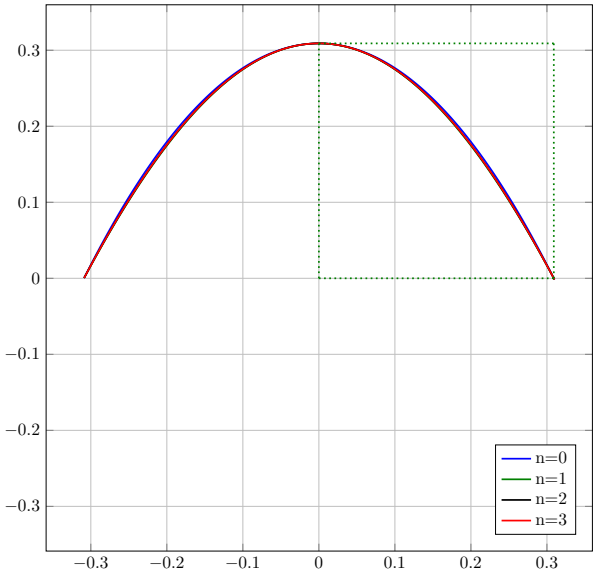
(A) f^9 with superstable 2 (B) f^{18} with superstable 2 (C) f^{36} with superstable 2

FIGURE 21. The Period Doubling Mechanism for 9_1

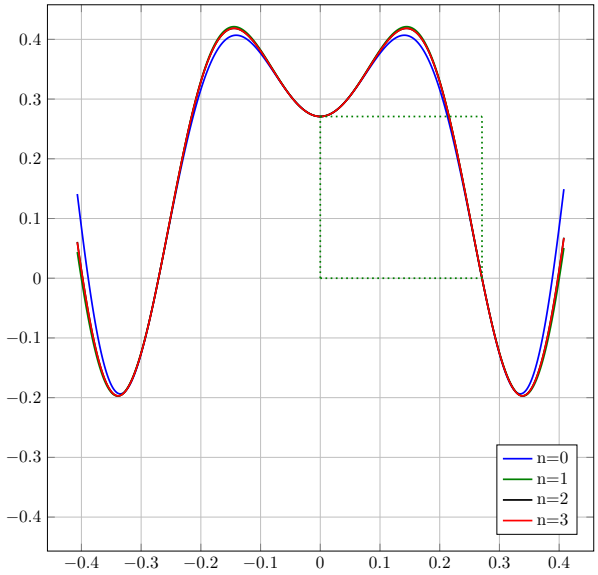


(A) f^9 with superstable 2 (B) f^{18} with superstable 2 (C) f^{36} with superstable 2

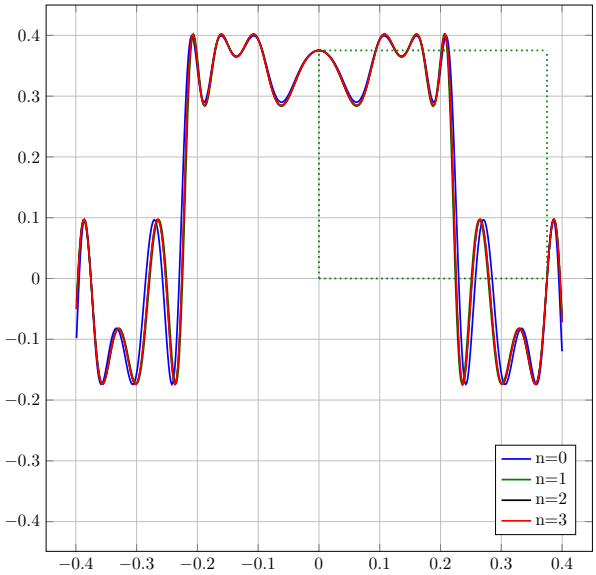
FIGURE 22. The Period Doubling Mechanism for 9_2



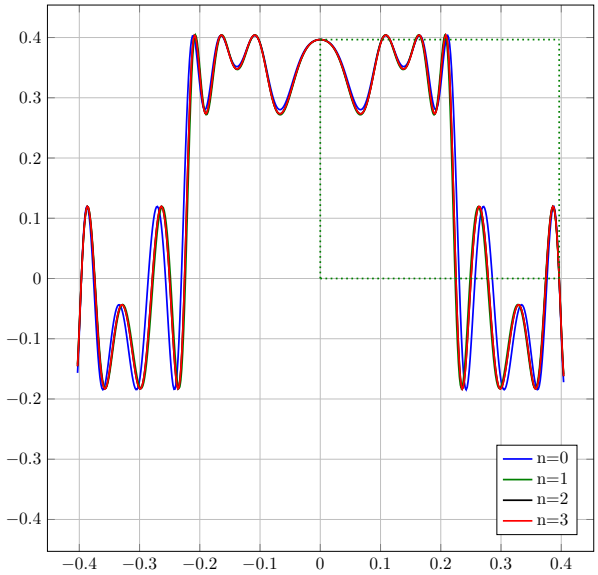
(A) Universal function g_1 for Period 2^n,
$g_1 = \lim_{n\to\infty} (-\alpha)^n f^{2^n}_{\lambda_{n+1}}\left(\frac{x}{(-\alpha)^n}\right)$



(B) Universal function g_1 for Period $3 \cdot 2^n$,
$g_1 = \lim_{n\to\infty} (-\alpha)^n f^{3_1\cdot 2^n}_{\lambda_{n+1}}\left(\frac{x}{(-\alpha)^n}\right)$

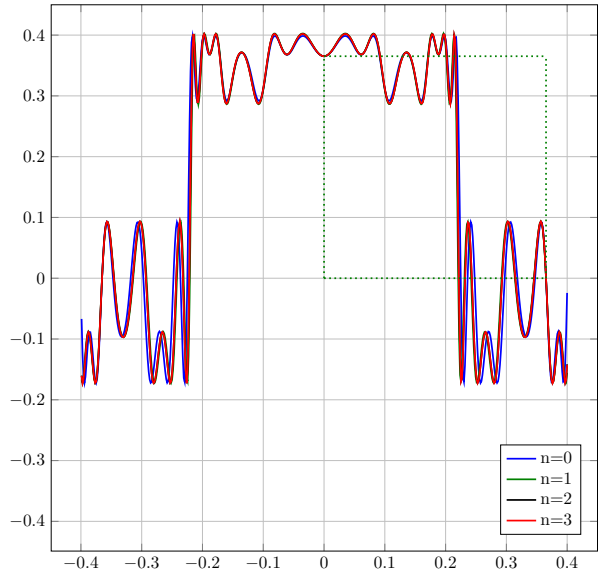


(C) Universal function g_1 for Period $7_1 \cdot 2^n$,
$g_1 = \lim_{n\to\infty} (-\alpha)^n f^{7_1\cdot 2^n}_{\lambda_{n+1}}\left(\frac{x}{(-\alpha)^n}\right)$

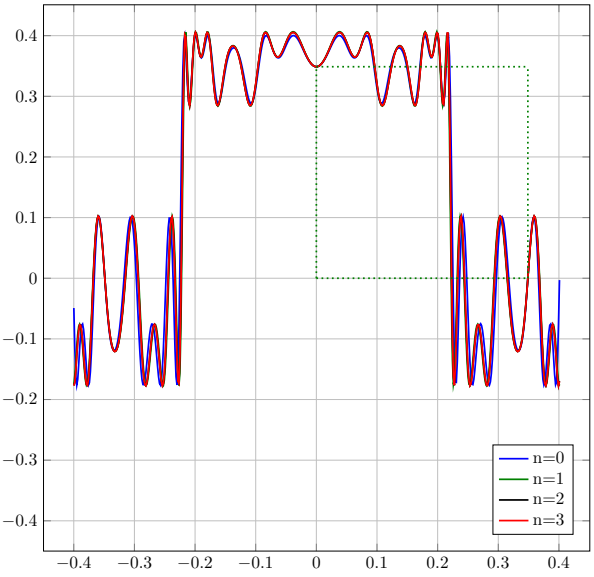


(D) Universal function g_1 for Period $7_2 \cdot 2^n$,
$g_1 = \lim_{n\to\infty} (-\alpha)^n f^{7_2\cdot 2^n}_{\lambda_{n+1}}\left(\frac{x}{(-\alpha)^n}\right)$

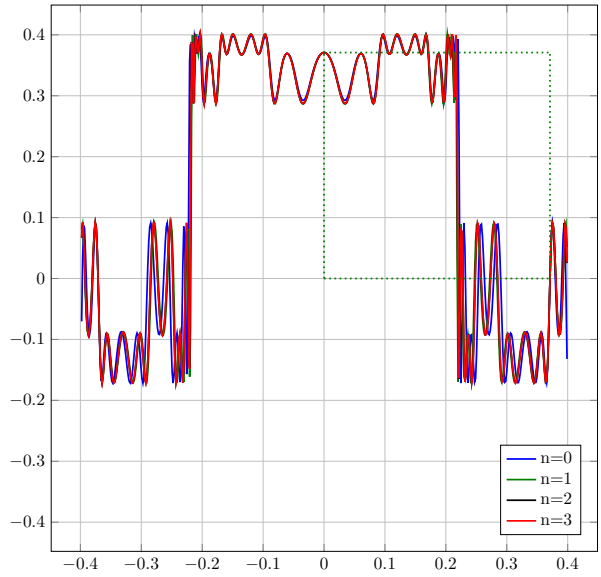
FIGURE 23. Universal Function g_1 for first appearance odds, Logistic Map.



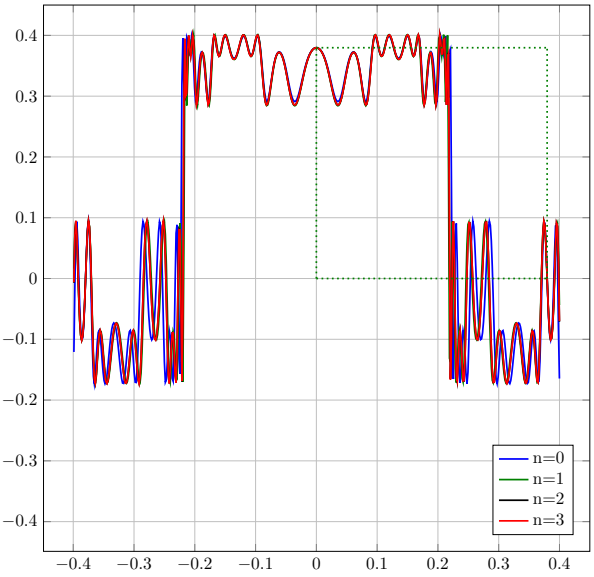
(A) Universal function g_1 for Period $9_1 \cdot 2^n$,
$g_1 = \lim_{n\to\infty} (-\alpha)^n f_{\lambda_{n+1}}^{9_1 \cdot 2^n}\left(\frac{x}{(-\alpha)^n}\right)$



(B) Universal function g_1 for Period $9_2 \cdot 2^n$,
$g_1 = \lim_{n\to\infty} (-\alpha)^n f_{\lambda_{n+1}}^{9_2 \cdot 2^n}\left(\frac{x}{(-\alpha)^n}\right)$

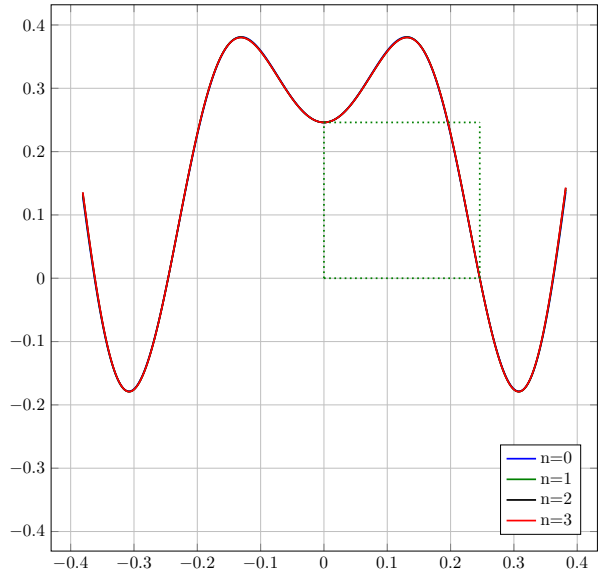


(C) Universal function g_1 for Period $11_1 \cdot 2^n$,
$g_1 = \lim_{n\to\infty} (-\alpha)^n f_{\lambda_{n+1}}^{11_1 \cdot 2^n}\left(\frac{x}{(-\alpha)^n}\right)$

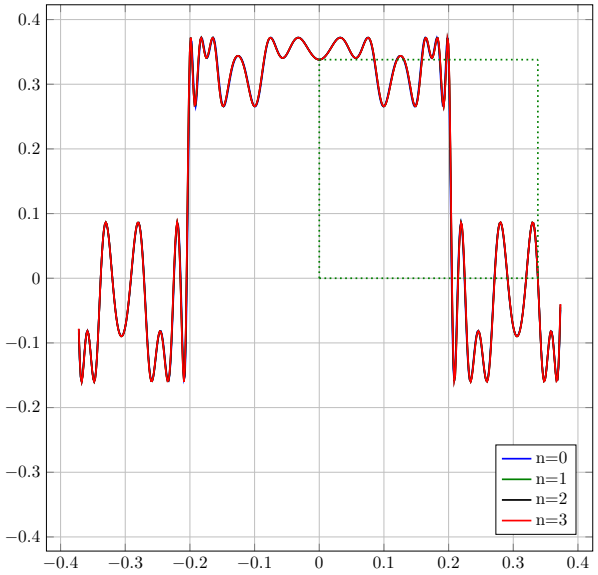


(D) Universal function g_1 for Period $11_2 \cdot 2^n$,
$g_1 = \lim_{n\to\infty} (-\alpha)^n f_{\lambda_{n+1}}^{11_2 \cdot 2^n}\left(\frac{x}{(-\alpha)^n}\right)$

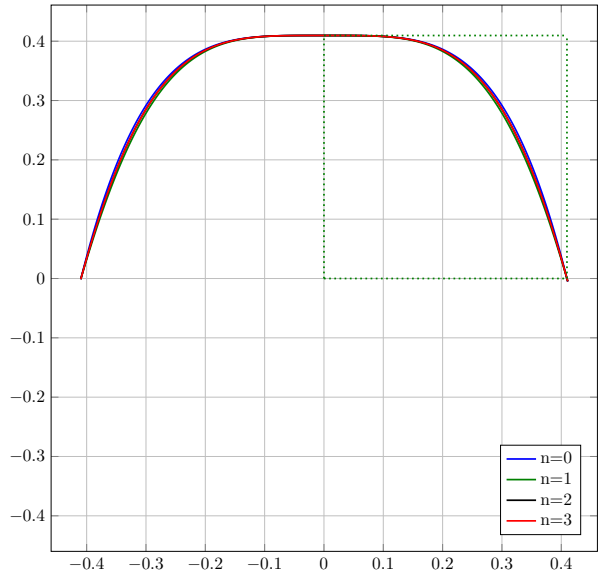
FIGURE 24. Universal Function g_1 for first appearance odds, Logistic Map.



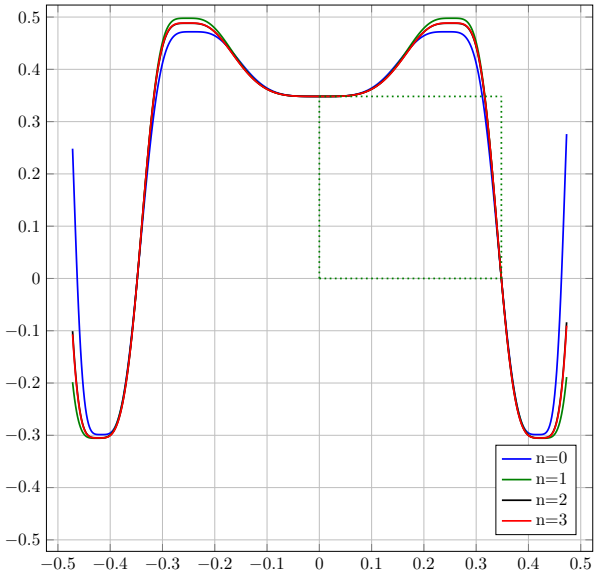
(A) Universal function g_1 for Period $3_1 \cdot 2^n$, $g_1 = \lim_{n\to\infty} (-\alpha)^n f^{3_1 \cdot 2^n}_{\lambda_{n+1}}\left(\frac{x}{(-\alpha)^n}\right)$, Sine map.



(B) Universal function g_1 for Period $9_1 \cdot 2^n$, $g_1 = \lim_{n\to\infty} (-\alpha)^n f^{9_1 \cdot 2^n}_{\lambda_{n+1}}\left(\frac{x}{(-\alpha)^n}\right)$, Sine map.



(C) Universal function g_1 for Period 2^n, $g_1 = \lim_{n\to\infty} (-\alpha)^n f^{2^n}_{\lambda_{n+1}}\left(\frac{x}{(-\alpha)^n}\right)$, Quartic map.



(D) Universal function g_1 for Period $3_1 \cdot 2^n$, $g_1 = \lim_{n\to\infty} (-\alpha)^n f^{3_1 \cdot 2^n}_{\lambda_{n+1}}\left(\frac{x}{(-\alpha)^n}\right)$, Quartic map.

FIGURE 25. Universal Function g_1 for first appearance odds, Sine and Quartic Maps.

5. Conclusions

The following are the main conclusions of this paper:

- We indroduced the notion of a second minimal orbit with respect to the Sharkovski ordering, for continuous endomorphisms on the real line. It is proved that there are 9-types of second minimal orbits up to their inverses. It is conjectured that there are $4k-3$-types of second minimal $(2k+1)$-orbits, with accuracy up to their inverses. The proof of this conjecture is addressed in a forthcoming paper.
- We demonstrate the numerical results which reveal a fascinating universal pattern of the distribution of periodic orbits within the chaotic regime of the bifurcation diagram of the one-parameter family of unimodal maps, when the parameter changes in the range between the Feigenbaum transition point to chaos and the value when the superstable 3-orbit appears for the first time. Numerical results demonstarte that this parameter range is divided into infinitely many Sharkovski s-blocks where all the $2^s(2k+1)$-orbits are distributed and the pattern is independent of s.
- The first appearance of any orbit in the indicated parameter range is always a minimal orbit [1]. Numerical results of this paper demonstrate that the second appearances of all odd orbits are always second minimal orbits with a Type 1 digraph. The reason for the relevance of exactly Type 1 second minimal (2k+1)-orbits are hidden in the fact that the topological structure of the single maximum unimodal map is equivalent to the topological structure of the piecewise monotonic map associated with Type 1 second minimal (2k+1)-orbits.
- Numerical results demonstrate that the convergence of the successive parameter values for superstable $2^s(2k+1)$-orbits within each s-block is exponential with a rate independent of the appearance index. In particular, for any fixed two appearance indices, the ratio of distances of parameter values for respective appearances of superstable $2^s(2k+1)$-orbits is asymptotically constant for large k. Otherwise speaking, there is an asymptotically constant shift in appearances.
- Numerical results demonstrate that any superstable odd orbits in the indicated parameter range are going through successful period doublings, according to the Feigenbaum scenario when the parameter decreases to the critical transition point. In particular, this reveals that the Feigenbaum universality is true in very general classes of maps, such as the class of maps which are the $(2k+1)$st iteration of the class of $\mathscr{C}^1$-unimodal maps. This generalization is a driving force of infinitely many Feigenbaum scenarios of transition to chaos through successive bifurcations of all possible odd orbits in the indicated range when the parameter decreases towards the first transition value to chaos.
- This paper outlines the elements of the rigorous Feigenbaum universality theory in the general class of maps, which are the $(2k+1)$st iteration of the class of $\mathscr{C}^1$-unimodal maps.

Acknowledgement

This research was funded by National Science Foundation: grant #1359074–REU Site: Partial Differential Equations and Dynamical Systems at Florida Institute of Technology (Principal Investigator Ugur G. Abdulla). Students Andy Ruden, Batul Kanawati (REU-2014), Alyssa Turnquist (REU-2015) and Emily Ribando-Gros (REU-2016) participated and contributed to numerical calculation of the superstable periodic orbits of the four model examples reported in the paper.

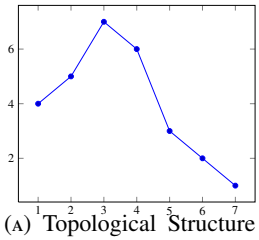
References

[1] A. U. Abdulla, R. U. Abdulla, and U. G. Abdulla, *On the minimal* $2(2k+1)$*-orbits of the continuous endomorphisms on the real line with application in chaos theory*, Journal of Difference Equations and Applications, 19 (2013), pp. 1395–1416.

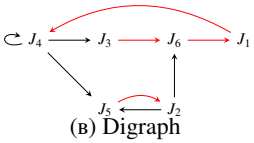
[2] L. Alseda, J. Llibre, and R. Serra, *Minimal periodic orbits for continuous maps of the interval*, Transactions of the American Mathematical Society, 286 (1984), pp. 595–627.

[3] L. Block and W. Coppel, *Stratification of continuous maps of an interval*, Transactions of the American Mathematical Society, 297 (1986), pp. 587–604.
[4] L. Block and W. A. Coppel, *Dynamics in One Dimension*, Springer-Verlag, 1992.
[5] L. Block, J. Guckenhimer, M. Misiurewicz, and L. Young, *Periodic points and topological entropy of one dimensional maps*, in Proceedings of the International Conference on Global Theory of Dynamical Systems, 1979, pp. 18–34.
[6] M. Campanino and H. Epstein, *On the existence of feigenbaum's fixed point*, Communications in Mathematical Physics, 79 (1981), pp. 261–302.
[7] P. Collet and J.-P. Eckmann, *Iterated maps on the interval as dynamical systems*, Birkhauser, Boston, 1980.
[8] P. Collet, J.-P. Eckmann, and O. Lanford, *Universal properties of maps on an interval*, Communications in Mathematical Physics, 76 (1980), pp. 211–254.
[9] M. Feigenbaum, *Quantitative universality for a class of nonlinear transformations*, Journal of Statistical Physics, 19 (1978), pp. 25–52.
[10] M. Feigenbaum, *The universal metric properties of nonlinear transformations*, Journal of statisical physics, 21 (1979), pp. 669–706.
[11] M. Feigenbaum, *Universal behavior in nonlinear systems*, Physica, 7D (1983), pp. 16–39.
[12] O. E. Lanford, *Remarks on the accumulation of period-doubling bifurcations*, in Mathematical problems in theoretical physics, Proceedings of The International Conference Mathematics and Physics 1979, Springer, 1980, pp. 340–342.
[13] N. Metropolis, M. L. Stein, and P. Stein, *On finite limit sets for transformations on the unit interval*, Journal of Combinatorial Theory, 15 (1973), pp. 25–44.
[14] J. Milnor and W. Thurston, *On iterated maps of the interval*, Dynamical Systems, 1342 (1988), pp. 465–563.
[15] A. Sharkovsky, *Coexistence of cycles of a continuous transofrmation of a line into itself*, Ukrains'kii Mathematical Zhurnal, 16 (1964), pp. 61–71.
[16] P. Stefan, *A theorem of Sharkovskii on the existence of periodic orbits of continuous endomorphisms of the real line*, Communications in Mathematical Physics, 54 (1977), pp. 237–248.
[17] P. D. Straffin, *Periodic points of continuous functions*, Mathematics Magazine, 51 (1978), pp. 99–105.

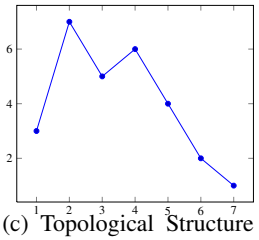
Appendix A. Topological Structure and Digraphs of Second Minimal 7 Periodic Orbits



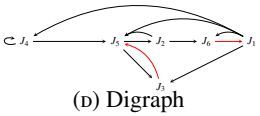
(A) Topological Structure 1: max



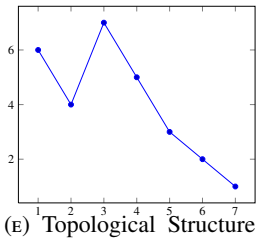
(B) Digraph



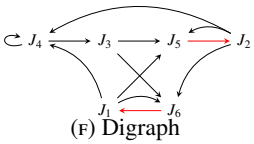
(C) Topological Structure 2: max-min-max



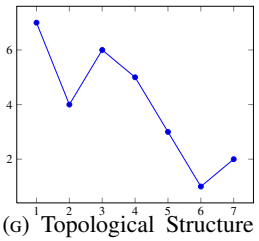
(D) Digraph



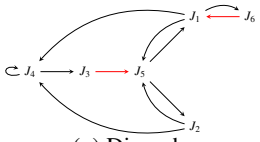
(E) Topological Structure 3: min-max



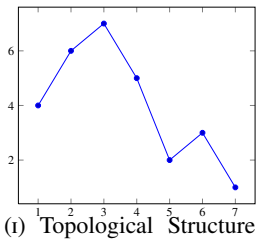
(F) Digraph



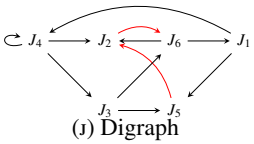
(G) Topological Structure 4: min-max-min



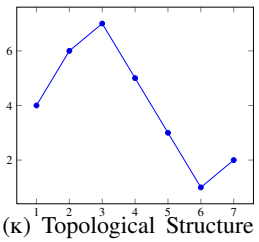
(H) Digraph



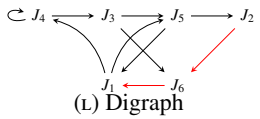
(I) Topological Structure 5: max-min-max



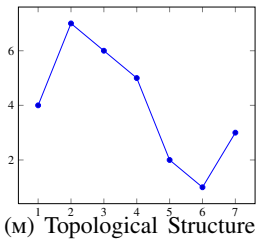
(J) Digraph



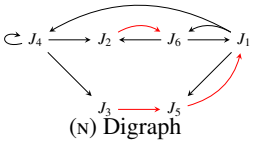
(K) Topological Structure 6: max-min



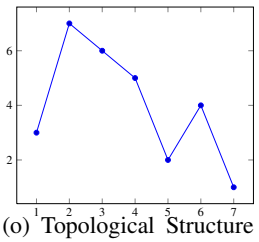
(L) Digraph



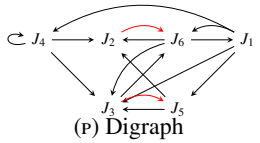
(M) Topological Structure 7: max-min



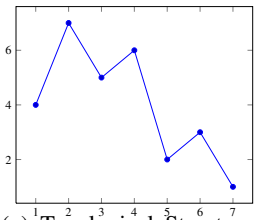
(N) Digraph



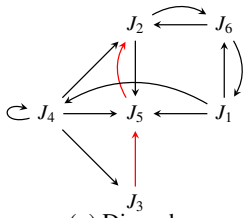
(O) Topological Structure 8: max-min-max



(P) Digraph



(Q) Topological Structure 9: max-min-max-min-max



(R) Digraph

Appendix B. Period Doubling Universality

Table 4. Logistic Map, Calculation of δ, α and λ_∞ for Period Doubling Starting at $(2k+1)_j$-orbit.

s	$(2^s(2k+1))_j$	$\delta = \frac{\lambda_{s-1,j}^{2k+1} - \lambda_{s-2,j}^{2k+1}}{\lambda_{s,i}^{2k+1} - \lambda_{s-1,j}^{2k+1}}$	$\frac{d_{s-1,j}^{2k+1}}{d_{s,j}^{2k+1}}$	$\lambda_\infty = \frac{\lambda_{s,j}^{2k+1} - \lambda_{s-1,j}^{2k+1}}{\delta} + \lambda_{s,j}^{2k+1}$
0	3_1			
1	6_1		−2.454268432041252	0.895949796617074064169461813134 87
2	12_1	4.507542941	−2.488688613626316	0.893130507974499054843099381538 67
3	24_1	4.695932444	−2.499742045692276	0.892627503175731617232828014629 88
4	48_1	4.667366742	−2.502259346885118	0.892516581647856875387279527735 07
0	5_1			
1	10_1		−2.461541495514402	0.894196999657421199197517978755 5
2	20_1	4.797049170	−2.491558266385502	0.892897154998874097294399540158 05
3	40_1	4.657504624	−2.500470850008986	0.892573415108649922808237905299 33
4	80_1	4.671681878	−2.502380674035116	0.892505087850642211812031720375 47
0	7_1			
1	14_1		−2.476379655788202	0.893712717699261242618837156410 13
2	28_1	4.878393687	−2.493625548299273	0.892805447413363086327552217053 84
3	56_1	4.647942857	−2.499064991443559	0.892553476641469571316506542445 97
4	112_1	4.673628954	−2.499927161986120	0.892500818551486331292485335875 11
0	7_2			
1	14_2		−2.441360908576077	0.894789721892727741843456033948 86
2	28_2	4.686149745	−2.488711635264935	0.892985307416590610373482188047 23
3	56_2	4.671758208	−2.499866778948107	0.892593414422730374906861654661 47
4	112_2	4.669957285	−2.502262858497064	0.892509344986931098030197627522 48
0	9_2			

1	18_2		−2.482362906116526	0.893906532525196636213888976984 9
2	36_2	4.843746928	−2.490050317301194	0.892843227579704668636153774068 62
3	72_2	4.652331109	−2.501126509692929	0.892561675616793168360961489650 78
4	144_2	4.671925051	-2.502292842294823	0.892502572049979313009862403682 01
0	11_2			
1	22_2		−2.493231131576156	0.893633224981802049777640312267 99
2	44_2	4.879885441	−2.491347078570966	0.892785218163614578323451879271 46
3	88_2	4.648157894	−2.501549958092916	0.892549219339056173052871832318 95
4	176_2	4.672309401	−2.502583102468284	0.892499903728947389699494209769 01

TABLE 5. Sine Map, Calculation of δ, α and λ_∞ for Period Doubling Starting at $(2k+1)_j$-orbit.

s	$(2^s(2k+1))_j$	$\delta = \frac{\lambda_{s-1,j}^{2k+1} - \lambda_{s-2,j}^{2k+1}}{\lambda_{s,i}^{2k+1} - \lambda_{s-1,j}^{2k+1}}$	$\frac{d_{s-1,j}^{2k+1}}{d_{s,j}^{2k+1}}$	$\lambda_\infty = \frac{\lambda_{s,j}^{2k+1} - \lambda_{s-1,j}^{2k+1}}{\delta} + \lambda_{s,j}^{2k+1}$
0	3_1			
1	6_1		−2.458609821276883	0.868739610509804522739819317368 55
2	12_1	4.730427896	−2.492752378392625	0.866278587174810518115201366035 87
3	24_1	4.689585511	−2.500535459353473	0.865730971002356934271212919377 19
4	48_1	4.673272858	−2.502381199234309	0.865611839262845641151779376821 67
0	5_1			
1	10_1		−2.469638603784021	0.867535667146893603527143890161 32
2	20_1	4.729401371	−2.495394712087649	0.866014873064077496304632536774 85
3	40_1	4.680960160	−2.501268413804899	0.865673237570861737059193192896 25
4	80_1	4.671707451	−2.502538204015066	0.865599424267684310258031976034 23
0	7_1			
1	14_1		−2.478098385927731	0.867094770119878826017780506488 16
2	28_1	4.723917393	−2.497172992020666	0.865915995565403581797939491583 51
3	56_1	4.677996484	−2.501655211509605	0.865651771728976230019574876376 71
4	112_1	4.671133912	−2.502632946021479	0.865594814856126726606444624025 38
0	7_2			
1	14_2		−2.458318467171219	0.867978197470521406487822791622 78
2	28_2	4.731506379	−2.493322400484982	0.866112990071415072476914532856 09
3	56_2	4.684043797	−2.500817171563748	0.865694629949226127705741903727 51

4	112_2	4.672304839	−2.502470979507185	0.865604022585592912815981558026 08
0	9_2			
1	18_2		−2.473348814781689	0.867276079741179529050465318285 77
2	36_2	4.726421035	−2.496081537357099	0.865956688443777966225732950121 07
3	72_2	4.679197352	−2.501449848132213	0.865660595069574073206397749740 63
4	144_2	4.671371561	−2.502598648169756	0.865596709349743479865641465764 37
0	11_2			
1	22_2		−2.478761450016932	0.867001299947878303564962798592 69
2	44_2	4.721501647	−2.497198146435454	0.865894754084838496779128812216 41
3	88_2	4.677401460	−2.501644350274001	0.865647172648607415653725829833 76
4	176_2	4.671023240	−2.502808956533517	0.865593828101172260605174817335 85

TABLE 6. Cubic Map, Calculation of δ, α and λ_∞ for Period Doubling Starting at $(2k+1)_j$-orbit.

s	$(2^s(2k+1))_j$	$\delta = \frac{\lambda_{s-1,j}^{2k+1} - \lambda_{s-2,j}^{2k+1}}{\lambda_{s,i}^{2k+1} - \lambda_{s-1,j}^{2k+1}}$	$\frac{d_{s-1,j}^{2k+1}}{d_{s,j}^{2k+1}}$	$\lambda_\infty = \frac{\lambda_{s,j}^{2k+1} - \lambda_{s-1,j}^{2k+1}}{\delta} + \lambda_{s,j}^{2k+1}$
0	7_2			
1	14_2		−2.372145654798267	0.888047892144962253969974501386 14
2	28_2	4.723797089	−2.531319536769563	0.886570749237654263507646506770 41
3	56_2	4.679053349	−2.485852964973201	0.886240115616404772081794628827 97
4	112_2	4.671403318	−2.508524126657965	0.886168790543695415532125379543 7
0	9_2			
1	18_2		−2.392012536453845	0.887527213580539121989385244649 42
2	36_2	4.68688313	−2.529350970159389	0.886446621759376648802685985987 09
3	72_2	4.677220605	−2.488427281068384	0.886213316613562735064969850703 65
4	144_2	4.670698719	−2.507942183936122	0.886163037352742614041727410032 16
0	11_2			
1	22_2		−2.401139119219189	0.887308622900223643534634708385 54
2	44_2	4.676860906	−2.528386409182592	0.886397671578413504750291947486 52
3	88_2	4.676259561	−2.489467206157571	0.886202749991492800742148124666 81
4	176_2	4.670438970	−2.507685078672229	0.886160770188904633111992432909 13
0	9_3			
1	18_3		−2.554658949633893	0.887930162591959212728460498924 83
2	36_3	4.68688313	−2.458084127102111	0.886541545233927020866199865403 02

3	72_3	4.677220605	−2.515688945322818	0.886233810299219833039696378518 15
4	144_3	4.671226897	−2.496763200983061	0.886167435556630802753544124074 28
0	11_3			
1	22_3		−2.552146100063579	0.887466197459942153763137383844 34
2	44_3	4.682776145	−2.464930838112400	0.886432579660219438001013474339 79
3	88_3	4.67700628	−2.514465146334054	0.886210286780477463877032775792 42
4	176_3	4.670623793	−2.497475746154126	0.886162386842111219545959497469 9
0	13_3			
1	26_3		−2.551864737909594	0.887282310562069854305598344189 61
2	52_3	4.675899873	−2.467548655440053	0.886391875935698223215318705696 61
3	104_3	4.67613272	−2.513787216936584	0.886201499725043587365243282965 78
4	208_3	4.670402066	−2.497175141254314	0.886160502153869742751583509829 72

TABLE 7. Quartic Map, Calculation of δ, α and λ_∞ for Period Doubling Starting at $(2k+1)_j$-orbit.

s	$(2^s(2k+1))_j$	$\delta = \frac{\lambda_{s-1,j}^{2k+1} - \lambda_{s-2,j}^{2k+1}}{\lambda_{s,i}^{2k+1} - \lambda_{s-1,j}^{2k+1}}$	$\frac{d_{s-1,j}^{2k+1}}{d_{s,j}^{2k+1}}$	$\lambda_\infty = \frac{\lambda_{s,j}^{2k+1} - \lambda_{s-1,j}^{2k+1}}{\delta} + \lambda_{s,j}^{2k+1}$
0	7_2			
1	14_2		−1.685016151822741	0.967953941593045057109385901816 54
2	28_2	7.257463741	−1.689616004337216	0.968526618360710930939478800074 75
3	56_2	7.286379135	−1.690226809471704	0.968606644767139293657158440522 14
4	112_2	7.284942740	−1.690235270778622	0.968617620189867714190278280780 51
0	9_2			
1	18_2		−1.706637878653648	0.968106224143703292858750498280 89
2	36_2	8.011416641	−1.686501852919600	0.968571200795980083235062153426 65
3	72_2	7.142547386	−1.691119908779726	0.968612150987261927359051885544 91
4	144_2	7.310491719	−1.689505962339770	0.968618391065218389579904153621 58
0	11_2			
1	22_2		−1.707417466698786	0.968203551540253786460364792811 96
2	44_2	8.104519001	−1.686805041920849	0.968581894453594255827546173469 14
3	88_2	7.12879172	−1.691103312794999	0.968613703158636793083307370840 34
4	176_2	7.313150062	−1.687906060312480	0.968618602047287554789025822075 86
0	9_3			

1	18_3		−1.691326896602970	0.967960236178453850633514102413 39
2	36_3	7.442423313	−1.688539412451539	0.968536941665751971090397191781 52
3	72_3	7.248421264	−1.690519553189105	0.968607799872997311410469800370 75
4	144_3	7.292133658	−1.690006740550708	0.968617785913796999359545196797 43
0	11_3			
1	22_3		−1.708260498375539	0.968123088428292246495513910100 4
2	44_3	8.094606895	−1.686293933989813	0.968574497170453428208628203456 68
3	88_3	7.127647184	−1.691037152267567	0.968612580041209807028001026242 12
4	176_3	7.313418511	−1.692380649828639	0.968618450582314993954854785096 06
0	13_3			
1	26_3		−1.707280529206626	0.968212260513517623760854812750 83
2	52_3	8.103299085	−1.686936763535888	0.968582650657597217019034539664 9
3	104_3	7.129597110	−1.691348289167268	0.968613819950728853852261628501 49
4	208_3	7.313591663	−1.678694125925514	0.968618618728068148739058922783 21

Appendix C. Parameter Tables

The following few pages contain parameter values that we used to construct the tables and figures in this document. Below is a key outlining the table headers.

- **Parameter**: the numeric value of the parameter for the associated map
- **P**: the super stable periodic orbit corresponding to the above parameter value
- **A**: the appearance number of the periodic orbit corresponding to the parameter value

TABLE 8. Parameter Values for Logistic Map $f_\lambda(x) = 4\lambda x(1-x)$

Parameter	P	A
0.5	1.0	1.0
0.8090169943749475	2.0	1.0
0.8746404248319252	4.0	1.0
0.8886602156922059	8.0	1.0
0.8916668449640671	16.0	1.0
0.8925435410844437	176.0	1.0
0.8925462153481506	144.0	1.0
0.8925493727315035	176.0	2.0
0.8925536426542862	112.0	1.0
0.8925582633384074	176.0	3.0
0.8925618374268403	144.0	2.0
0.8925652869739683	176.0	4.0
0.892573585	80.0	1.0
0.892582971578052	176.0	5.0
0.8925860303078793	144.0	3.0
0.8925889559052782	176.0	6.0
0.8925934776392263	112.0	2.0
0.8925977476162251	176.0	7.0
0.8926000233456378	144.0	4.0
0.8926020087836917	176.0	8.0
0.8926169497695979	176.0	9.0
0.8926273	48.0	1.0
0.8926273095473648	144.0	5.0
0.8926424478626298	144.0	6.0
0.8926468116175647	176.0	10.0
0.8926516782349787	176.0	11.0
0.8926574315669168	144.0	7.0
0.8926586161442951	176.0	12.0
0.8926614251928092	112.0	3.0
0.8926652649929492	144.0	8.0
0.8926842268307457	112.0	4.0
0.8926913356572714	144.0	9.0
0.892695290032331	144.0	10.0
0.8926999134097414	144.0	11.0
0.8927022801053289	112.0	5.0
0.8927050057536571	144.0	12.0
0.8927172512571973	112.0	6.0
0.8927293163954468	112.0	7.0
0.8927391046311725	112.0	8.0
0.892745143089132	112.0	9.0
0.8927531275154216	88.0	1.0
0.892765612708715	72.0	1.0
0.8927803546566632	88.0	2.0
0.8928002912804274	56.0	1.0
0.8928218666978042	88.0	3.0
0.8928385565717427	72.0	2.0
0.8928546647294011	88.0	4.0
0.89286570826588	112.0	10.0
0.8928758764598548	112.0	11.0
0.892893412	40.0	1.0
0.8929185769659241	112.0	12.0
0.8929372464436822	88.0	5.0
0.892951531075995	72.0	3.0
0.892965194521167	88.0	6.0
0.8929863118792093	56.0	2.0
0.8930062532268376	88.0	7.0
0.8930168810677759	72.0	4.0
0.8930261525483736	88.0	8.0
0.8930959299227967	88.0	9.0
0.893144323	24.0	1.0
0.8932150514348008	72.0	5.0
0.8932354347086963	88.0	10.0
0.8932581641927477	88.0	11.0
0.8932657490534088	88.0	12.0
0.8932850347611261	72.0	6.0
0.8933036890878607	56.0	3.0
0.8933216260408074	72.0	7.0
0.8933978510203553	72.0	8.0
0.8934102079449422	56.0	4.0
0.8934213197439284	72.0	9.0
0.8934434098714304	72.0	10.0
0.8934618867418858	72.0	11.0
0.8934834850666612	72.0	12.0
0.8934945442626503	56.0	5.0
0.8935645266299209	56.0	6.0
0.8936209165390675	56.0	7.0
0.8936666925819085	56.0	8.0
0.893694946890496	56.0	9.0

Parameter	P	A	Parameter	P	A
0.8937323239550504	44.0	1.0	0.8985555274564071	18.0	1.0
0.8937906969816722	36.0	1.0	0.8988759584501568	22.0	2.0
0.8938595743690791	44.0	2.0	0.8993095495931392	14.0	1.0
0.8939527169808105	28.0	1.0	0.8993368709151569	28.0	10.0
0.8939585734139139	56.0	10.0	0.8997801682018646	22.0	3.0
0.8940534775173637	44.0	3.0	0.900145977896958	18.0	2.0
0.8941313720345442	36.0	2.0	0.9004988403933514	22.0	4.0
0.8942065586523593	44.0	4.0	0.900739199236906	28.0	11.0
0.894258151388425	56.0	11.0	0.9009615610934926	28.0	12.0
0.894387542	20.0	1.0	0.9013464593838434	10.0	1.0
0.8945920053348253	44.0	5.0	0.9023089359519223	22.0	5.0
0.8946586324286321	36.0	3.0	0.9026237070977975	18.0	3.0
0.8947223418891009	44.0	6.0	0.9029255119168045	22.0	6.0
0.894820829737213	28.0	2.0	0.9033912545246447	14.0	2.0
0.8949138449982476	44.0	7.0	0.9038307061198744	22.0	7.0
0.8949634233198132	36.0	4.0	0.9040647384776517	18.0	4.0
0.8950067008708713	44.0	8.0	0.904267999021263	22.0	8.0
0.8953321587557187	44.0	9.0	0.904899707989313	16.0	3.0
0.8955574589550901	12.0	1.0	0.9058068890614333	22.0	9.0
0.8955574589550902	36.0	5.0	0.9068893823788807	6.0	1.0
0.8958862652026675	36.0	6.0	0.907823200062555	12.0	2.0
0.8959812147446011	44.0	10.0	0.9084892763171067	18.0	5.0
0.8960872008248462	44.0	11.0	0.908943552643572	22.0	10.0
0.8961224931207159	44.0	12.0	0.909446366503746	22.0	11.0
0.896187724634684	44.0	13.0	0.9095331442064777	16.0	4.0
0.8962125114340377	36.0	7.0	0.909616877636151	22.0	12.0
0.8962994172610155	28.0	3.0	0.9099232980258403	22.0	13.0
0.8963829388112704	36.0	8.0	0.9100404763587777	18.0	6.0
0.8967376720178901	36.0	9.0	0.9104560684602736	14.0	3.0
0.8967952385115885	28.0	4.0	0.9108571928810814	18.0	7.0
0.8968470365678113	36.0	10.0	0.9113101549515245	16.0	5.0
0.8969500795862201	36.0	11.0	0.9117622003804752	10.0	2.0
0.8970359452655111	36.0	12.0	0.9122196907504082	16.0	6.0
0.8971364940346715	36.0	13.0	0.9125698915821074	18.0	8.0
0.8971878607732342	28.0	5.0	0.9128454558604397	14.0	4.0
0.897349960937811	16.0	2.0	0.9130921658581117	18.0	9.0
0.8975119706948392	28.0	6.0	0.9133219453957768	16.0	7.0
0.897773472481103	28.0	7.0	0.913580229382562	18.0	10.0
0.8979846837132985	28.0	8.0	0.9137869897027185	12.0	3.0
0.8981144866729309	28.0	9.0	0.9140000120689893	18.0	11.0
0.898285536828268	22.0	1.0	0.9142572545642417	16.0	8.0

Parameter	P	A	Parameter	P	A
0.9144843071853473	18.0	12.0	0.9198101479894252	23.0	3.0
0.9147365695291755	14.0	5.0	0.9198106458924652	33.0	3.0
0.9150310389753986	18.0	13.0	0.9198220811388089	17.0	2.0
0.9155481259216439	8.0	2.0	0.9198265854125903	27.0	3.0
0.9156307240370415	16.0	9.0	0.919864618020104	19.0	3.0
0.9163686307982645	14.0	6.0	0.9199002311171905	29.0	4.0
0.9167444770891021	16.0	10.0	0.9199010748389	31.0	4.0
0.9170937820054763	12.0	4.0	0.919902361355556	23.0	4.0
0.9174080707508858	16.0	11.0	0.9199062616676469	27.0	4.0
0.9176716828336033	14.0	7.0	0.919909788780055	25.0	4.0
0.9179438449410644	16.0	12.0	0.9199257014200635	13.0	1.0
0.918252061590967	10.0	3.0	0.9199604232996532	33.0	4.0
0.9185479687517751	16.0	13.0	0.9199641405971246	21.0	4.0
0.9187709570364896	14.0	8.0	0.9199901616901687	19.0	4.0
0.9189599787371455	16.0	14.0	0.9200000703977084	27.0	5.0
0.9191588201786222	12.0	5.0	0.9200028110917958	23.0	5.0
0.9193383506312537	16.0	15.0	0.9200076215315786	25.0	5.0
0.9194727761973615	14.0	9.0	0.9200103594866011	33.0	5.0
0.9195830311115901	16.0	16.0	0.9200106468302367	31.0	5.0
0.9196435795904915	27.0	1.0	0.9200112670767221	29.0	5.0
0.9196439467055643	25.0	1.0	0.9200132410614315	21.0	5.0
0.919644981018353	23.0	1.0	0.9200389918663741	17.0	3.0
0.9196457756192704	31.0	1.0	0.9200856001137521	19.0	5.0
0.9196459733265683	33.0	1.0	0.9201002143603496	33.0	6.0
0.919646584854938	29.0	1.0	0.9201016145225464	29.0	6.0
0.9196478947752951	21.0	1.0	0.9201028782109886	25.0	6.0
0.9196561008171046	19.0	1.0	0.9201090481341733	21.0	6.0
0.9196791956839688	17.0	1.0	0.9201105233194542	31.0	6.0
0.9197000311872442	33.0	2.0	0.9201219025506991	23.0	6.0
0.9197006174971487	29.0	2.0	0.9201255900181393	27.0	6.0
0.9197013110760547	27.0	2.0	0.9201422993862319	15.0	2.0
0.9197027892812369	25.0	2.0	0.9202001209047099	33.0	7.0
0.9197070458081346	19.0	2.0	0.9202005092526497	31.0	7.0
0.9197149184463773	23.0	2.0	0.9202028502440535	19.0	6.0
0.919720432954781	31.0	2.0	0.9202076590267333	27.0	7.0
0.9197223223802037	21.0	2.0	0.9202106868115649	25.0	7.0
0.9197440854758494	15.0	1.0	0.9202121549955485	29.0	7.0
0.9198001163269032	29.0	3.0	0.9202163098045701	23.0	7.0
0.9198006805909831	31.0	3.0	0.9202278551537337	21.0	7.0
0.9198015834347826	21.0	3.0	0.9202587007006321	17.0	4.0
0.9198060374454656	25.0	3.0	0.9203000082728384	33.0	8.0

Parameter	P	A	Parameter	P	A
0.9203010086311395	29.0	8.0	0.9208098673955014	19.0	10.0
0.9203057998429245	23.0	8.0	0.9208136718855724	29.0	13.0
0.9203127589957107	25.0	8.0	0.9208200470149717	33.0	12.0
0.9203165520944553	27.0	8.0	0.9208239900768528	23.0	13.0
0.9203227908438997	19.0	7.0	0.9208357735776028	21.0	12.0
0.920342369174139	31.0	8.0	0.9208669721008041	17.0	6.0
0.9203571728536436	21.0	8.0	0.9209010909575819	33.0	13.0
0.9204296685342831	11.0	1.0	0.9209014409363525	31.0	14.0
0.9204767917194359	31.0	9.0	0.9209022018802908	29.0	14.0
0.9204782548259948	27.0	9.0	0.9209065639725457	25.0	14.0
0.9204811789142139	25.0	9.0	0.9209125024919976	23.0	14.0
0.9204886765851206	23.0	9.0	0.9209159028698781	27.0	14.0
0.920491177506046	29.0	9.0	0.9209285533727417	19.0	11.0
0.9205005434280713	27.0	10.0	0.9209609162728946	21.0	13.0
0.9205016326349753	31.0	10.0	0.9210201003306971	13.0	2.0
0.9205060640270746	21.0	9.0	0.9210523200855003	29.0	15.0
0.9205100093913368	33.0	9.0	0.9210565730461244	25.0	15.0
0.9205152878078745	25.0	10.0	0.921060891466536	31.0	15.0
0.9205204912373594	29.0	10.0	0.9210642268502021	23.0	15.0
0.9205229230057148	23.0	10.0	0.9210684773689786	27.0	15.0
0.9205419557953939	19.0	8.0	0.9210811677775855	21.0	14.0
0.9206005784482749	31.0	11.0	0.9210906606157544	33.0	14.0
0.9206016043882802	27.0	11.0	0.9211005911749909	33.0	15.0
0.9206035067349837	29.0	11.0	0.9211045739676469	25.0	16.0
0.9206106074930887	17.0	5.0	0.9211102289158498	29.0	16.0
0.9206233780780297	25.0	11.0	0.9211152051517735	19.0	12.0
0.9206307692696445	23.0	11.0	0.9211323778639362	23.0	16.0
0.9206445592873718	21.0	10.0	0.9211358613331826	27.0	16.0
0.9206503319730334	33.0	10.0	0.9211463306470374	21.0	15.0
0.9206722630021638	19.0	9.0	0.9211500728400285	31.0	16.0
0.920701250060699	21.0	11.0	0.9211820874871725	17.0	7.0
0.9207028636238962	33.0	11.0	0.9212003053975469	33.0	16.0
0.9207058521120631	27.0	12.0	0.9212007128291876	29.0	17.0
0.9207091690061839	25.0	12.0	0.9212015158659378	31.0	17.0
0.9207108947869364	29.0	12.0	0.9212029872773682	23.0	17.0
0.9207162655093767	23.0	12.0	0.9212066360711628	27.0	17.0
0.9207419764574405	15.0	3.0	0.9212095811496441	25.0	17.0
0.9207611508956879	31.0	12.0	0.9212170738871973	21.0	16.0
0.9208003677980954	31.0	13.0	0.9212463984436541	19.0	13.0
0.9208013027396837	25.0	13.0	0.921300240890266	33.0	17.0
0.9208044399266484	27.0	13.0	0.9213006615814194	29.0	18.0

Parameter	P	A	Parameter	P	A
0.9213014802403597	31.0	18.0	0.9220230674037606	23.0	22.0
0.9213026978247993	25.0	18.0	0.9220360043243131	21.0	20.0
0.92130631826283	27.0	18.0	0.9220694892396009	19.0	16.0
0.9213262606625509	15.0	4.0	0.9221006939816137	33.0	25.0
0.9213588721853865	23.0	18.0	0.9221048175786382	21.0	21.0
0.9213762639622086	21.0	17.0	0.9221120027015463	29.0	24.0
0.9214035603610099	27.0	19.0	0.9221139584364046	25.0	23.0
0.9214107783908108	19.0	14.0	0.9221218006952228	23.0	23.0
0.9214153297683447	31.0	19.0	0.922126355265872	27.0	23.0
0.9214200902652883	33.0	18.0	0.9221480960567324	17.0	9.0
0.9214216285362573	25.0	19.0	0.922159726448752	31.0	25.0
0.9214288350417134	23.0	19.0	0.9222002247854527	33.0	26.0
0.9214310694267652	29.0	19.0	0.9222005785028199	29.0	25.0
0.9214438552596709	21.0	18.0	0.9222011980332242	31.0	26.0
0.9214845277144422	17.0	8.0	0.9222057411189049	23.0	24.0
0.9215001291474537	33.0	19.0	0.9222129968030404	25.0	24.0
0.9215010171790381	25.0	20.0	0.9222166052355004	27.0	24.0
0.9215049782513212	27.0	20.0	0.9222244298335882	19.0	17.0
0.9215095294630585	23.0	20.0	0.9222597382550419	21.0	22.0
0.9215112716081109	31.0	20.0	0.9223138550089415	15.0	5.0
0.9215121500634174	29.0	20.0	0.9223381697320739	29.0	26.0
0.9215262948579038	21.0	19.0	0.9223393802222187	27.0	25.0
0.9215608336278994	19.0	15.0	0.922342562851247	25.0	25.0
0.9216002756249053	33.0	20.0	0.9223501969457514	23.0	25.0
0.9216008621175658	25.0	21.0	0.9223519582560188	31.0	27.0
0.9216017202012348	31.0	21.0	0.9223665449604025	21.0	23.0
0.921606307688425	23.0	21.0	0.922399214446316	19.0	18.0
0.9216126226488097	27.0	21.0	0.922406402226228	27.0	26.0
0.921753409712203	31.0	22.0	0.9224096209205783	25.0	26.0
0.9217577448964835	29.0	21.0	0.9224112875747574	29.0	27.0
0.9217611380044505	33.0	21.0	0.9224161022741247	23.0	26.0
0.921804045233538	9.0	1.0	0.9224297139943903	21.0	24.0
0.9218590865036999	33.0	22.0	0.9224411422767945	31.0	28.0
0.9218641957928685	31.0	23.0	0.9224669462877152	17.0	10.0
0.9218709393905855	29.0	22.0	0.9225049540612161	21.0	25.0
0.9219718987947105	33.0	23.0	0.9225111577683214	29.0	28.0
0.9220111472734216	33.0	24.0	0.9225127813206834	25.0	27.0
0.9220160672052569	29.0	23.0	0.9225156274141197	27.0	27.0
0.9220166608744411	27.0	22.0	0.9225191563794206	23.0	27.0
0.9220183435162941	25.0	22.0	0.92253694125618	19.0	19.0
0.9220208907672919	31.0	24.0	0.922542458896398	31.0	29.0

Parameter	P	A	Parameter	P	A
0.9226176193928061	31.0	30.0	0.9232037853402316	25.0	33.0
0.9226464425273783	13.0	3.0	0.9232113433701622	21.0	31.0
0.9226985119519096	27.0	28.0	0.9232159122244098	27.0	34.0
0.9227008178525822	25.0	28.0	0.9233553354446671	11.0	2.0
0.9227022407363636	29.0	29.0	0.9234364494843212	29.0	35.0
0.922703450274448	27.0	29.0	0.9234875471606739	25.0	34.0
0.9227069440391705	23.0	28.0	0.9234952282874029	27.0	35.0
0.9227218838495027	21.0	26.0	0.923505076081172	21.0	32.0
0.92275449593336	19.0	20.0	0.9235127679201179	25.0	35.0
0.9227598793106112	31.0	31.0	0.9235155521191672	27.0	36.0
0.9228004001233571	31.0	32.0	0.9235372401278704	19.0	24.0
0.9228055063846784	25.0	29.0	0.9236101303997307	17.0	13.0
0.9228208374473782	17.0	11.0	0.9236248828050347	27.0	37.0
0.9228318593515585	29.0	30.0	0.9236279066755088	25.0	36.0
0.9228424021108256	23.0	29.0	0.9236491052579816	21.0	33.0
0.9228457697436099	27.0	30.0	0.9236796161121292	19.0	25.0
0.9228555496778423	21.0	27.0	0.9237031728677695	25.0	37.0
0.9228834258451859	19.0	21.0	0.9237111298598573	21.0	34.0
0.9229008001875197	31.0	33.0	0.9237162552841238	27.0	38.0
0.9229053068625388	25.0	30.0	0.9237638529359127	15.0	7.0
0.9229128243166754	21.0	28.0	0.9238051113914373	27.0	39.0
0.9229176329559665	27.0	31.0	0.9238079477611446	25.0	38.0
0.9229222384020115	29.0	31.0	0.9238158785374112	21.0	35.0
0.9229271234309651	23.0	30.0	0.9238460988672327	19.0	26.0
0.9229611968821689	15.0	6.0	0.9239112916557798	17.0	14.0
0.9230008998938598	29.0	32.0	0.9239255388317077	27.0	40.0
0.9230025440384575	25.0	31.0	0.9239488116172666	21.0	36.0
0.923005640632976	27.0	32.0	0.9239796821838245	19.0	27.0
0.9230106288246114	21.0	29.0	0.9240118642346291	21.0	37.0
0.9230134345245601	31.0	34.0	0.9240168986630016	27.0	41.0
0.9230246352291566	23.0	31.0	0.9240988760780329	13.0	4.0
0.9230414320248848	19.0	22.0	0.9241659057686024	27.0	42.0
0.923108777775757	17.0	12.0	0.9241874953823742	21.0	38.0
0.9231208724973803	31.0	35.0	0.9242056864820108	27.0	43.0
0.9231213450951792	29.0	33.0	0.9242202029150759	19.0	28.0
0.9231257848675283	25.0	32.0	0.9242516437364504	21.0	39.0
0.923132894975511	23.0	32.0	0.9242901169978515	17.0	15.0
0.9231366730398138	27.0	33.0	0.9243274730242318	21.0	40.0
0.9231477692758365	21.0	30.0	0.9243566357281391	19.0	29.0
0.9231797780922061	19.0	23.0	0.924440039748957	15.0	8.0
0.9232022555173477	29.0	34.0	0.9244925837164232	21.0	41.0

Parameter	P	A	Parameter	P	A
0.9245216932198678	19.0	30.0	0.9295822427339708	16.0	20.0
0.9245488951118092	21.0	42.0	0.9298079717433595	17.0	25.0
0.9245822242032017	17.0	16.0	0.9299278057808813	15.0	13.0
0.9246362004773152	19.0	31.0	0.9300482202563531	17.0	26.0
0.9248291259456144	16.0	17.0	0.9302132331790187	13.0	7.0
0.9254422883844889	7.0	1.0	0.9303744281142803	17.0	27.0
0.9255708476075072	14.0	10.0	0.9304878779751862	15.0	14.0
0.9261810653663104	16.0	18.0	0.9306020957994455	17.0	28.0
0.9263695549335671	19.0	32.0	0.9308659010883394	11.0	4.0
0.926422205650506	17.0	17.0	0.9311266981784078	17.0	29.0
0.926480708392207	19.0	33.0	0.931234015921366	15.0	15.0
0.9265617938148366	15.0	9.0	0.9313370849667829	17.0	30.0
0.9266443295176789	19.0	34.0	0.9314786851600155	13.0	8.0
0.9267072296096274	17.0	18.0	0.9316127851041636	17.0	31.0
0.9267719927018105	19.0	35.0	0.9316990324815639	15.0	16.0
0.9268990591234583	13.0	5.0	0.931774933086075	17.0	32.0
0.9270246251963171	19.0	36.0	0.931881041671243	16.0	21.0
0.9270866574862666	17.0	19.0	0.9320175871084143	14.0	11.0
0.9271462242414003	19.0	37.0	0.9321798504486302	16.0	22.0
0.9272250976785409	15.0	10.0	0.9324535237980285	12.0	6.0
0.92730477980184	19.0	38.0	0.9327763934958844	16.0	23.0
0.9273649682044417	17.0	20.0	0.9330334577962366	14.0	12.0
0.9274246529676042	19.0	39.0	0.9333315218062391	16.0	24.0
0.927643837998337	11.0	3.0	0.9336982614806218	17.0	33.0
0.9278623135222064	19.0	40.0	0.9347287282426712	5.0	1.0
0.9279189741782298	17.0	21.0	0.9354619793333402	10.0	4.0
0.9279752930366489	19.0	41.0	0.936004218370594	15.0	17.0
0.9280495878140084	15.0	11.0	0.9365481090303157	17.0	34.0
0.9281221075383218	19.0	42.0	0.9368470960303923	16.0	25.0
0.9281752606494361	17.0	22.0	0.9371045687350086	14.0	13.0
0.9282295925464943	19.0	43.0	0.9373251521199856	16.0	26.0
0.92834448677078	13.0	6.0	0.9375492280855212	17.0	35.0
0.928460602487508	19.0	44.0	0.9376188083061392	12.0	7.0
0.9285154193462041	17.0	23.0	0.9376870171464302	17.0	36.0
0.9285688582630766	19.0	45.0	0.9378666057635101	16.0	27.0
0.9286415302414859	15.0	12.0	0.9380019767238563	14.0	14.0
0.9287139150577448	19.0	46.0	0.938117088017013	16.0	28.0
0.928765286070779	17.0	24.0	0.9382016815414446	17.0	37.0
0.9288127175465508	19.0	47.0	0.9382639401482904	15.0	18.0
0.9289968814034584	16.0	19.0	0.9383328148965207	17.0	38.0
0.9292792068508622	9.0	2.0	0.938448694765481	13.0	9.0

Parameter	P	A	Parameter	P	A
0.938569177987284	17.0	39.0	0.9430870153972655	16.0	37.0
0.9386465789836986	15.0	19.0	0.9435535472252282	7.0	2.0
0.9387244096568935	17.0	40.0	0.9436340122846377	14.0	18.0
0.9388708890819253	16.0	29.0	0.9440868779686737	16.0	38.0
0.9389691251075292	11.0	5.0	0.9442804882592601	17.0	55.0
0.9390695421382402	16.0	30.0	0.944400441261753	12.0	9.0
0.9392151036120271	17.0	41.0	0.9445048407326306	17.0	56.0
0.9392926094377416	15.0	20.0	0.9446182118866014	16.0	39.0
0.9393698233226494	17.0	42.0	0.9447209484546417	14.0	19.0
0.9394928977047089	13.0	10.0	0.9448077454709249	16.0	40.0
0.9396153225473503	17.0	43.0	0.9448674903684716	17.0	57.0
0.939690024842712	15.0	21.0	0.9449126279511749	15.0	26.0
0.9397608915679229	17.0	44.0	0.9449612825801651	17.0	58.0
0.9398638787402191	16.0	31.0	0.9450488345622481	13.0	13.0
0.9400376250602329	14.0	15.0	0.9451381264415866	17.0	59.0
0.9403137986767697	9.0	3.0	0.9451899365694643	15.0	27.0
0.94059942667533	14.0	16.0	0.9452412487095767	17.0	60.0
0.9407653946677715	16.0	32.0	0.9453222087248859	16.0	41.0
0.9408613682291624	17.0	45.0	0.9454345985777954	11.0	7.0
0.9409270154265458	15.0	22.0	0.9455471174411741	16.0	42.0
0.9409953129169278	17.0	46.0	0.9456259644051741	17.0	61.0
0.9411078240980755	13.0	11.0	0.9456755743657617	15.0	28.0
0.941219364734741	17.0	47.0	0.9457253447634651	17.0	62.0
0.9412866882425523	15.0	23.0	0.9458115547312089	13.0	14.0
0.9413532521023238	17.0	48.0	0.9458967766826185	17.0	63.0
0.9414673057559139	16.0	33.0	0.9459443478465995	15.0	29.0
0.9415765699409272	11.0	6.0	0.9459893788372576	17.0	64.0
0.9416867792979688	16.0	34.0	0.9460505092541333	16.0	43.0
0.9417978781941158	17.0	49.0	0.9461476071342457	14.0	20.0
0.9418617516317436	15.0	24.0	0.9462966096162295	16.0	44.0
0.9419252584019139	17.0	50.0	0.9464449481328123	9.0	4.0
0.9420287698786108	13.0	12.0	0.9465988685328639	16.0	45.0
0.9421288573690431	17.0	51.0	0.9467408391711305	14.0	21.0
0.942185810613247	15.0	25.0	0.9468310268519844	16.0	46.0
0.9422379080085772	17.0	52.0	0.9468864578791083	17.0	65.0
0.9423072956256685	16.0	35.0	0.9469269490048738	15.0	30.0
0.942405302536878	14.0	17.0	0.9469691298705613	17.0	66.0
0.9425207052272616	16.0	36.0	0.9470443898694233	13.0	15.0
0.9426527498373356	17.0	53.0	0.9471188724630772	17.0	67.0
0.9427557608876059	12.0	8.0	0.9471603042130635	15.0	31.0
0.9428743623740117	17.0	54.0	0.9472008999953558	17.0	68.0

Parameter	P	A	Parameter	P	A
0.9472621657601605	16.0	47.0	0.9505347418045125	17.0	82.0
0.9473591815013696	11.0	8.0	0.9506352651907028	15.0	38.0
0.9474541321755662	16.0	48.0	0.9507189563549525	17.0	83.0
0.9475106957943875	17.0	69.0	0.9508487313327707	13.0	18.0
0.9475469696260843	15.0	32.0	0.9509575188358351	17.0	84.0
0.9476448977552586	13.0	16.0	0.9510088573843923	15.0	39.0
0.9477034426138526	17.0	70.0	0.9510544395866831	17.0	85.0
0.947733921617124	15.0	33.0	0.9511093923830842	16.0	58.0
0.9477966857540892	16.0	49.0	0.9511864043035728	14.0	26.0
0.9478462851458759	14.0	22.0	0.9512673274850394	16.0	59.0
0.9479006922691185	16.0	50.0	0.9513363596128612	17.0	86.0
0.9479516033174422	17.0	71.0	0.9514221837472476	12.0	12.0
0.9480053188877896	12.0	10.0	0.9515089240660483	17.0	87.0
0.9480607439004328	17.0	72.0	0.9515790930715127	16.0	60.0
0.9481160741636439	16.0	51.0	0.9516631530453461	14.0	27.0
0.9481796300838617	14.0	23.0	0.9517463040461553	16.0	61.0
0.9482435763382607	16.0	52.0	0.951808892592533	17.0	88.0
0.9482944689150308	17.0	73.0	0.9518652770653788	15.0	40.0
0.9483413732621206	15.0	34.0	0.9519383831319697	17.0	89.0
0.948408642108592	17.0	74.0	0.9521244725098057	10.0	6.0
0.9485164441889147	10.0	5.0	0.9523162411492646	17.0	90.0
0.9486285476412364	17.0	75.0	0.9523905365647094	15.0	41.0
0.9486987975767931	15.0	35.0	0.9524481238036833	17.0	91.0
0.9487487242954044	17.0	76.0	0.9525120069820141	16.0	62.0
0.9488036471569236	16.0	53.0	0.9525975616461875	14.0	28.0
0.9488743597460321	14.0	24.0	0.9526840291164363	16.0	63.0
0.9489462845704794	16.0	54.0	0.9527546685675844	17.0	92.0
0.949009332533322	17.0	77.0	0.9528475463736816	12.0	13.0
0.9490780804877298	12.0	11.0	0.9529398694971234	17.0	93.0
0.9491473662644617	17.0	78.0	0.9530080745662677	16.0	64.0
0.9492107277102163	16.0	55.0	0.9530891576691004	14.0	29.0
0.9492826687713001	14.0	25.0	0.9531651619914416	16.0	65.0
0.9493514336511595	16.0	56.0	0.9532174331812081	17.0	94.0
0.9494014907276402	17.0	79.0	0.9532603361848672	15.0	42.0
0.9494428882786827	15.0	36.0	0.9533072546905522	17.0	95.0
0.9495891122434322	13.0	17.0	0.9534043196366604	13.0	19.0
0.9497094552611501	17.0	80.0	0.9535088561007298	17.0	96.0
0.9497890939253142	15.0	37.0	0.9535658791619818	15.0	43.0
0.9498857281645797	17.0	81.0	0.9536237513110958	17.0	97.0
0.9501927359686673	8.0	3.0	0.9537070876960089	16.0	66.0
0.9502236731934814	16.0	57.0	0.9539187227353836	11.0	9.0

Parameter	P	A
0.9541535736642798	16.0	67.0
0.9542576473407822	17.0	98.0
0.9543353288341542	15.0	44.0
0.9544165158088548	17.0	99.0
0.9545820065186768	13.0	20.0
0.9547587014626097	17.0	100.0
0.954852987166387	15.0	45.0
0.9549467352368605	17.0	101.0
0.9550714036503227	16.0	68.0
0.9552867504518042	14.0	30.0
0.9555838961047767	16.0	69.0
0.9559280829047855	17.0	102.0
0.9579685138208287	3.0	1.0